

# Mtss1 promotes maturation and maintenance of cerebellar neurons via splice variant-specific effects

Thorsten Sistig<sup>1</sup> · Fanziska Lang<sup>1</sup> · Sebastian Wrobel<sup>1</sup> · Stephan L. Baader<sup>1</sup> · Karl Schilling<sup>1</sup> · Britta Eiberger<sup>1</sup>

Received: 15 April 2016 / Accepted: 17 January 2017 / Published online: 18 February 2017  
© Springer-Verlag Berlin Heidelberg 2017

**Abstract** Efficient coupling of the actin cytoskeleton to the cell membrane is crucial for histogenesis and maintenance of the nervous system. At this critical interface, BAR (Bin–Amphiphysin–Rvs) proteins regulate membrane bending, shown to be instrumental for mobility and morphogenesis of individual cells. Yet, the systemic significance of these proteins remains largely unexplored. Here, we probe the role of a prominent member of this protein family, the inverse-BAR protein Mtss1, for the development and function of a paradigmatic neuronal circuit, the cerebellar cortex. Mtss1-null mice show granule cell ectopias, dysmorphic Purkinje cells, malformed axons, and a protracted neurodegeneration entailing age-dependent motor deficits. In postmitotic granule cells, which transiently express Mtss1 while they migrate and form neurites, Mtss1 impinges on directional persistence and neuritogenesis. The latter effect can be specifically attributed to its exon 12a splice variant. Targeted re-expression of Mtss1 in Mtss1-null animals indicated that these pathologies were largely due to cell type-specific and intrinsic effects. Together, our results provide a mechanistic perspective on

Mtss1 function for brain development and degeneration and relate it to structural features of this protein.

**Keywords** Actin cytoskeleton · Cell migration · Neuritogenesis · Neurodegeneration

## Introduction

A characteristic of the vertebrate central nervous system (CNS) is that most of its constituent cells originate far from where they reside in the adult. Consequently, developing nerve cells have to faithfully navigate a complex and dynamically changing environment to assure the proper formation of a functional CNS (e.g., Rakic 1988; Metin et al. 2008; Marin and Rubenstein 2003). Further, nerve cells may also be distinguished from non-neuronal cells as they establish extensive connections with cells well beyond the immediate neighborhood of their own somata.

Cell membrane dynamics is central to these key developmental processes as well as to the adult function and maintenance of neural circuitry. Changes in cell shape concomitant with differentiation, cellular motility, and polarization all go along with plasmalemma remodeling and require its integration with cell-extrinsic signals and intracellular structure, notably the actin cytoskeleton. Consequently, proteins that couple membrane dynamics to that of actin filaments have attracted considerable attention (Flynn 2013; Da Silva and Dotti 2002).

Mtss1 is a prominent member of this functional group widely expressed in the developing nervous system (Mattila et al. 2003; Hayn-Leichsenring et al. 2011; Saarikangas et al. 2015; and this paper). Its association with the cell membrane results in a characteristic negative membrane bending and the formation of protrusions linked to the actin

---

While this manuscript was under review, Yu et al. (Neuroscience, (2016) 333:123–131; doi: <http://dx.doi.org/10.1016/j.neuroscience.2016.07.002>) described differential effects of Mtss1 on axonal and dendritic growth in cultured granule cells that are fully consistent with our in vivo and in vitro observations.

---

**Electronic supplementary material** The online version of this article (doi:10.1007/s00429-017-1372-8) contains supplementary material, which is available to authorized users.

---

✉ Britta Eiberger  
britta.eiberger@uni-bonn.de

<sup>1</sup> Anatomisches Institut, Anatomie and Zellbiologie, University of Bonn, Nussallee 10, 53115 Bonn, Germany

cytoskeleton (for reviews, see e.g., Suetsugu 2010; Suetsugu et al. 2014). The gene-encoding *Mtss1* was observed early on to be differentially expressed in metastatic vs non-metastatic prostate cancer cells (Lee et al. 2002), and consequently suspected to play a role in cell motility. Since then, aberrant *Mtss1* expression has been observed in a variety of tumors (e.g., Dawson et al. 2012b; Mertz et al. 2014; Lei et al. 2014). During physiologic development, lack of *Mtss1* results in renal malfunction due to a compromised integrity of kidney epithelia intercellular junctions (Saarikangas et al. 2011; see also; Dawson et al. 2012a). *Mtss1* has also been shown to be necessary for spine formation in cerebellar Purkinje neurons (Saarikangas et al. 2015).

While these observations pinpoint the significance of *Mtss1* for normal tissue differentiation and maintenance and have revealed considerable molecular mechanistic insight (cf references above), we are still a far cry from a consistent view of how *Mtss1* may impinge on cellular integration and the development and maintenance of complex tissues. This is not least due to the rather widespread expression of *Mtss1*, in cells that differentiate interdependently or interact in mature tissues. Consequently, how aberrant *Mtss1* expression affects individual cells, and how this then translates into tissue dysfunction cannot be effectively deduced from scenarios characterized by global *Mtss1* dysregulation.

Here, we use the murine cerebellum as a model to address these issues. In the cerebellar cortex, *Mtss1* is expressed in Purkinje cells and, transiently during development, in differentiating granule neurons (Glassmann et al. 2007). The developmental history of these two cell types and their interdependence is known in exquisite detail (for reviews and further references, see Leto et al. 2016), and both are directly amenable to selective genetic manipulation (cf Oberdick et al. 1990; Ben-Arie et al. 1997). This allowed us to compare cellular and histogenetic effects of globally aberrant *Mtss1* expression with that in which either Purkinje neurons or granule cells were targeted selectively. As readout, we assessed migration and neurite formation, two key developmental steps dependent on membrane protrusion dynamics.

The findings presented allow to discern cell-specific and transcellular effects of *Mtss1* on cellular survival, motility, and process formation during development and maturation of a paradigmatic neural circuit. They identify a distinct role for the brain-specific exon 12a splice variant of *Mtss1* for neuritogenesis. Lastly, we document that *Mtss1*-related developmental defects eventually lead to age-dependent neurodegeneration and motor deficits. These data yield novel insights on how the actin- and membrane-binding protein *Mtss1* assures proper brain histogenesis and maintenance.

## Materials and methods

### Animals

*Mtss1*-KO mice were obtained from Dr. Rong Li, The Stowers Institute for Medical Research, Kansas City, MO, USA and have been described previously (Xia et al. 2010). All animals used for the present experiments were maintained on a mixed, predominantly C57/B16 genetic background. Mice were housed in temperature-, light-, and humidity-controlled rooms with a 12-h light/dark cycle. All animal handling was done in strict adherence to governmental (Directive 2010/63/EU of the European Parliament and of the Council of 22 September 2010) and institutional animal care regulations. Animals of either sex were used for the experiments except for the rotarod analyses where only males were investigated. Cell type-specific expression of *Mtss1* in Purkinje neurons or granule cells in a null background was achieved by crossing *Mtss1*-KO mice with *Pcp2(L7)*-cre (Barski et al. 2000) or *Atoh1(Math1)*-cre (Matei et al. 2005), respectively. Consequently, in double transgenic mice, the splicing of the endogenous 5' exon of *Mtss1* into the gene trapping cassette generating a fusion transcript of *Mtss1* and *lacZ* is suppressed, and the wild-type situation is restored.

### Tissue preparation and qPCR analysis

Total RNA was extracted from cerebella of P0, P8, and adult *Mtss1*-KO and age-matched control mice using Trizol reagent following the manufacturer's instructions (Life Technologies). The RNA was stored at  $-80^{\circ}\text{C}$ . RNA yield and quality were determined with a Qubit 2.0 Fluorometer (Life Technologies) and by agarose gel electrophoresis. Five  $\mu\text{l}$  of diluted RNA eluate (10 ng/ $\mu\text{l}$ ) was reverse-transcribed in 20  $\mu\text{l}$  reactions using the iScript cDNA Synthesis Kit (BioRad). The cDNA samples were stored at  $-20^{\circ}\text{C}$  in nuclease-free, low nucleic acid-binding microcentrifuge tubes. The cDNA was diluted to 2.5 ng/ $\mu\text{l}$  and assayed in 10  $\mu\text{l}$  PCR reactions. The sequence-specific Taqman primers for *Mtss1*-iso12 (Assay ID: Mm00460621\_m1) and *Mtss1*-iso12a (Mm01200879\_m1) were purchased from Life Technologies. GAPDH (Mm99999915\_g1) was used as a reference gene. A no-template control (NTC) of water was purified with the samples and profiled like the samples. Each gene was assayed on Bio-Rad Hard-Shell Plates (Bio-Rad, CA, USA) containing triplicate wells of cDNA from all samples. Each qPCR reaction contained the following: 5  $\mu\text{l}$  PCR master mix (TaqMan Gene Expression Master Mix, Life Technologies), 0.5  $\mu\text{l}$  of each primer set, and 3  $\mu\text{l}$  of cDNA. All qPCR reactions were carried out on CFX96 Touch Real-Time PCR Detection System (Bio-Rad). The thermal cycling parameters used were as follows: A 2-min

incubation at 50 °C and a 10-min initial denaturation at 95 °C, followed by 40 cycles of two-step amplification at 95 °C for 15 s and 60 °C for 60 s, and a final incubation for 30 s at 65 °C. PCR efficiency was determined from a standard curve. The correct size of the PCR products was confirmed by electrophoresis on a 2.5% agarose gel stained with ethidium bromide.

Technical replicates (triplicates) of C<sub>q</sub> values for each sample were combined in a single mean value and then further analyzed by the method of Pfaffl (2001). Expression levels are reported as relative to those of GAPDH. Experimental variability was calculated based on biological replicates.

## Histology

Mice were sacrificed by intraperitoneal injection of an overdose of anesthetic (a combination of ketamine hydrochloride and xylazine hydrochloride) and subsequent transcardial perfusion with 40 ml phosphate-buffered saline (PBS) followed by 25 ml 4% (w/v) freshly depolymerized paraformaldehyde (PFA) in PBS (150 mM NaCl, 10 mM Na<sub>2</sub>HPO<sub>4</sub>, pH 7.4). Brains were dissected from the mice and postfixed for 24 h in the same fixative. They were then extensively washed with tap water, dehydrated by passage through graded ethanols (30, 40, 50, 60, 70, 80, and 95%), and embedded in paraffin. Serial sections were cut in the sagittal plane at a thickness of 10 μm, rehydrated by standard procedures, and stained with 0.1% cresyl violet (Nissl staining).

For the preparation of cryosections, perfusion-fixed brains were postfixed in the same fixative for 30 min. They were then transferred to PBS containing 30% (w/v) glucose and incubated at 4 °C overnight. Subsequently, they were mounted in Tissue-Tek O.C.T. (Sakura Finetek) embedding medium. Cryosections were cut at 10 μm using a cryostat (HM560, Microm, Thermo Fisher Scientific).

## Immunostaining

Mice were perfused as described above. Brains were postfixed in 2% PFA for at least one week at 4 °C. Fifty-μm-thick free floating vibratome sections were obtained (VT 1200 S, Leica), and stained as described previously (Tress et al. 2011). As primary antibodies, mouse anti-NeuN antibodies (1:100, EMD Millipore, mouse monoclonal MAB377) were used to identify granule cells, and rabbit polyclonal anti-Calbindin antibodies (1:2000, Swant, CB38) were used for staining of cerebellar Purkinje cells. Antibodies detecting mouse Mtss1 splice isoforms were raised against the amino acid sequences CLPASRLLP RVTSVHLPD (Mtss1-iso12) and GSTMGAWVSTK (Mtss1-iso12a) after an epitope analysis by Thermo Fisher

Scientific and used in a dilution of 1:500. Binding of these antisera to tissue sections could be blocked with their specific immunogenic peptides. To further test the specificity of these antibodies, we generated GST fusion proteins incorporating the specific sequences of these exons. The following primers were used to amplify the corresponding gene regions by PCR: Ex12-BamHI: cgcggatccgGCTGCCAACCAGTTGTCTAA, Ex12-EcoRI: ggaattccggGTCATAGGGTCCTGGCTTTG, Ex12a-EcoRI: ggaattccggCTTTGCCAGTCCTTCTCTG, Ex12a-BamHI: cgggactcgcgGAAGCTGCCAACCAGAACTC. The resulting amplicons were cloned using the EcoRI and BamHI restriction sites into pGEX-6P-1 (GE Healthcare Life Sciences), which were then transfected into *E. coli* Rosetta cells (Invitrogen) using standard procedures. Bacterial lysates were subjected to western blot analysis and probed with anti-Mtss1-iso12 and anti-Mtss1-iso12a antibodies. Furthermore, mouse anti-GST antibodies (1: 1000, Sigma, 1160) were used to analyze the presence of the GST tag in all recombinant proteins. In western blots with tissue lysates of Mtss1-KO cerebella, neither anti-Mtss1-iso12 nor anti-Mtss1-iso12a antibodies revealed any signal at the molecular weight of Mtss1 (~110 kDa). The antibody to exon 12a, however, stained a few bands with molecular weights <50 kDa, both in tissue extracts from wild-type and Mtss1-deficient animals. To test whether this antibody may still be used to specifically detect Mtss1-exon 12 on tissue sections, we stained sections prepared from Mtss1-null animals with this antibody, and also that for exon 12a. In contrast to their intense staining of granule and/or Purkinje cells in cerebellar sections of wild-type animals (see, e.g., Fig. 8b), neither antibody resulted in any staining of these cells on sections from Mtss1-null animals (data not shown), documenting their specificity when used on formalin-fixed tissue sections.

For immunohistochemistry of paraffin-embedded material, rehydrated sections were heated to 94 °C in 10 mM sodium citrate buffer (pH 6.1) for 20 min. Endogenous peroxidase activity was blocked by incubation in 10% methanol/0.1% H<sub>2</sub>O<sub>2</sub> in PBS for 5 min. Sections were then incubated in 0.5% Triton X-100 in PBS for 15 min. Non-specific protein-binding sites were blocked by incubation with 2% normal serum in PBS for 1–2 h. Sections were then reacted with primary antibodies diluted in blocking reagent at 4 °C overnight.

When β-Gal histochemical and immunohistochemical analyses were combined, cryostat sections were fixed in 4% PFA for 5 min and subsequently incubated in a solution containing 5-bromo-4-chloro-3-indolyl-galactoside (X-gal) as described (Schilling et al. 1991b). For immunohistochemical analyses, β-Gal-stained sections were incubated in 10% methanol/0.1% H<sub>2</sub>O<sub>2</sub> / 90% PBS for 10 min to block endogenous peroxidase activity.

Afterwards, sections were permeabilized for 10 min in PBS containing 0.5% Triton X-100 and blocked by incubation in 2% normal serum from the species in which the secondary antibody had been generated. Primary and secondary antibodies were diluted in blocking solution. The following antibodies were used in this study: sheep polyclonal anti-Plexin B2 (1:20, R&D Systems, AF5329) and mouse monoclonal anti-NeuN (1:100, EMD Millipore).

For immunocytochemistry, cell cultures were fixed 48 h after plating with 4% PFA in PBS for 10 min. For X-gal histochemistry, fixed cells were stained for  $\beta$ -Gal activity as described (Schilling et al. 1991b). After a 30-min incubation with 2% normal goat serum to block free protein-binding sites, cultures were incubated overnight at 4 °C with primary antisera diluted in 2% normal goat serum. We used rabbit anti-MAP2 (1:1,000, Cell Signaling Technologies, 4542) to stain neurites. To analyze granule cell proliferation, a mouse anti-BrdU antibody (1:200, Sigma, B2531) was used.

The immunoreaction product was visualized using biotinylated secondary antibodies (goat anti-mouse, Vector Laboratories, BA-9200; goat anti-rabbit, Vector Laboratories, BA-1000) at a concentration of 1:200, and diaminobenzidine as a chromogen. For fluorescently labeled cultures, cells fixed and blocked as outlined above were stained with anti-MAP2 (1:1000), nuclei were visualized using Hoechst 33,258 dye (1  $\mu$ g/ml). After staining, cells were coverslipped and imaged (Axioskop 2, Axiovert 200 M, Zeiss).

To test for structural abnormalities of Purkinje cell dendrites, we counted spines on tertiary branchlets. Further, we assessed abnormal, downward orientation of main dendritic branches by counting numbers of dendrites that originated distal to the first dendritic branch point and intersected a line drawn parallel to the Purkinje cell layer end passing through this first branch point. A total of 36 Purkinje cells from wild-type and 33 cells from *Mtss1*-null cerebella were analyzed, drawn randomly from sections obtained from three different animals of either genotype. Results were compared using a G-test with William's correction.

To assess the extent of granule cell ectopias, we measured, in mid-sagittal sections of adult animals, the areas occupied by clusters of granule cells outside the internal granule cell layer. At least three animals null for *Mtss1*, with restored expression of *Mtss1* in Purkinje cells, or with restored expression in granule cell precursors were analyzed. Data were analyzed using Anova, and post hoc comparisons, we calculated using Tukey (all treatment) contrasts as implemented in the R package multcomp (Hothorn et al. 2008).

## Immunoblotting

For protein analysis, cerebella or cultured granule cells were solubilized in RIPA buffer supplemented with protease inhibitor cocktail (Complete, Roche Diagnostics) by sonification. A total of 25  $\mu$ g per sample was fractionated by SDS polyacrylamide gels and transferred to Immobilon-P PVDF membranes (Millipore) by semidry electro-transfer (BioRad). After blocking with 5% (w/v) non-fat dry milk in TBST (0.05 mM Tris, 0.150 mM NaCl, 0.05% (v/v) Tween20, pH 7.6), the membranes were incubated with the following antibodies: rabbit anti-*Mtss1* (1:125, Biomol, IMG-6108A), rabbit anti-*Mtss1*-iso12 (1:250), rabbit anti-*Mtss1*-iso12a (1:250), and rabbit anti-cyclophilin B (1:10,000, abcam, ab16045). After three washes for 5 min in TBST blots were incubated with HRP-conjugated goat anti-mouse (1:30,000, Dianova, 115-035-146) or goat anti-rabbit antibodies (1:30,000, Dianova, 111-035-144) for 2 h at 20 °C. Protein signal was visualized using the Super-Signal West Pico detection system (Pierce) according to the manufacturer's instructions.

## Golgi staining

To study the morphology of granule neurons in situ, we Golgi-impregnated adult cerebella of three *Mtss1*-KO and three wild-type littermates using the FD Rapid GolgiStain kit (FD Neurotechnologies) according to the manufacturer's recommendations. Granule neurons of lobus simplex were visualized using an Axioskop 2 microscope, and images were acquired with a Cool Snap EZ digital camera (Visitron Systems) and AxioVision 4.8.2.0 software (Carl Zeiss Microimaging GmbH). Images of Golgi-labeled cells were obtained using a *z*-stack of ten to twelve microphotographs taken at 1- $\mu$ m intervals throughout the slice and put into a single focused image with the software ImageJ 1.48.

## Culture of primary cerebellar granule cells

Primary dissociated cerebellar cells were prepared as described (Weisheit et al. 2006). Briefly, cerebella from eight-day-old postnatal mice were dissected in Hanks' balanced salt solution (modified to contain 4.17 mM  $\text{NaHCO}_3$  and 0.7 mM  $\text{Na}_2\text{HPO}_4 \cdot 2\text{H}_2\text{O}$ , pH 7.2), and the meninges were completely removed. The cerebella were mechanically dissociated in small pieces, which were then incubated with 0.05% trypsin/EDTA in PBS at 37 °C for 15 min. The trypsin action was stopped with trypsin inhibitor (Life Technologies) and the cell suspension was passed through a nylon mesh (pore size 250  $\mu$ m). Dissociated cells were pelleted by low-speed centrifugation. They were then resuspended in serum-free medium, and trypan blue-excluding cells were counted. Cells were grown at a

density of 500,000 cells/cm<sup>2</sup> on 24-well multidishes that had been coated overnight with poly-L-lysine (Sigma) and, subsequently, for 2 h at 37°C with laminin (Sigma). Cultures were maintained for 24 or 48 h at 37°C under 5% CO<sub>2</sub> in serum-free, B27-supplemented Neurobasal medium (Gibco).

### Time-lapse video microscopy

For time-lapse studies, cells were prepared and plated as described above. Four hours after plating, cultures were transferred to an incubator (5% CO<sub>2</sub>, 37°C, humidified) mounted on an inverted microscope (Leica DMIRE2) equipped with a digital CCD camera (DFC350FX, Leica). Bright-field images were recorded at low magnification (N-Plan 20x/0.04, Leica) with a sampling interval of 10 min during a total observation period of 280 min. To analyze cell mobility, 169 WT neurons and 172 KO neurons were tracked in cultures from three independent preparations (pooled cells from 2 mice each). Cell trajectories were determined by following the center of the granule cell using the ImageJ plugin ‘MTrackJ’ (<http://www.imagej-science.org/meijering/software/mtrackj/>). To characterize cell migration, the time-averaged mean square displacement was calculated for each track (MSD; cf Michalet 2010, formula 7). Linear fits to MSD values were based on intervals up to 150 min.

### BrdU incorporation

For the proliferation assay, primary granule cells were obtained as described above and grown in 24-well dishes (Nunc) in a volume of 100 µl and a concentration of 3 × 10<sup>5</sup> cells/ml. For Shh treatment, cells were incubated with 0.625 µg/ml of recombinant human Shh-N (R&D Systems) for 24 h. Subsequently, BrdU (Sigma), at 40 µM, was added to the media. After another four-hour-long incubation, cells were fixed (4% PFA). BrdU incorporation was monitored by immunostaining. All experiments were performed at least in triplicates.

Percentages of BrdU-positive cells were compared using a generalized linear model with a logit link. Genetic background and treatment were entered as predictive factors in the model. For post hoc comparisons, we calculated Tukey contrasts using the R package multcomp (Hothorn et al. 2008).

### Viral transduction of primary granule cells

For N-terminal Strep-tagging of Mtss1, full-length cDNAs of the Mtss1 isoforms comprising exon 12 or

exon 12a were cloned into the mammalian Step-tag vector pEXPR-IBA5 (IBA). The PCR products were subcloned in-frame with a Strep-tag into an AAV backbone containing the 1.1-kb CMV enhancer/chicken β-actin (CBA) promoter, the woodchuck posttranscriptional regulatory element (WPRE), and the bovine growth hormone polyA (AAV-iso12, AAV-iso12a). The same AAV-CBA-HA-WPRE-bGH backbone carrying the Tomato reporter gene was used as a control (AAV-control). AAV pseudotyped vectors (virions containing a 1:1 ratio of AAV1 and AAV2 capsid proteins with AAV2 ITRs) were generated as described (McClure et al. 2011). Briefly, human embryonic kidney 293 (HEK) cells were transfected with the AAV plasmid, the AAV1 (pH21) and AAV2 (pRV1) helper plasmids, and the adenovirus helper plasmid (pFΔ6, Stratagene) by standard calcium phosphate transfection methods. Forty-eight hours after transfection cells were harvested and lysed by four freeze/thaw cycles. The efficiency of the viral particles was tested by adding different amounts of HEK lysate to the cultures (four hours after plating) and analyzing the number of Strep-positive cells (anti-StrepMAB Classic, IBA, 2-1507-001). For all experiments, cultures with a transduction efficiency of at least 95% were used.

To analyze the effects of Mtss1-exon 12 and 12a variants on neurogenesis, we immunostained cultures transduced with the appropriate viral constructs for Map2 after six and ten days in vitro (DIV) as described above. As controls, we included non-transduced cultures derived from wild-type and Mtss1<sup>-/-</sup> mice. Randomly chosen areas were photographed using a 40x objective, and these micrographs were used for quantitative analysis. An estimate of cell density was obtained by counting cell nuclei. To assess neurite density, we quantified numbers of Map2-positive pixels, which is a function of neurite numbers, neurite length, and thickness (or the thickness of fasciculated neurites). We used ImageJ to first threshold the images (using the “mean” threshold implemented in ImageJ) and subsequently measured the fraction of immunoreactive pixels. This approach is preferable to direct morphometry of individual neurites, as these are typically tightly interwoven and fasciculated in high-density cultures as are needed to assure long enough survival for efficient viral expression. For statistical comparison of neurite density, we analyzed the data using a generalized linear model with a logit link to account for the fact that the response variable was on a proportional (percentage) scale. As predictor variable, we used the Mtss1-variant expressed (wild-type, exon 12, exon 12a, or none). Cell numbers were entered as a covariate (i.e., to control for variations in cell density). For post hoc comparisons, we calculated Tukey (all treatment) contrasts using the R package multcomp (Hothorn et al. 2008).

## Rotarod analysis

Motor coordination and balancing were tested with an accelerating rotarod (Ugo Basile). During the acquisition phase, each mouse was given three trials (with an intertrial interval of  $\geq 25$  min to control for possible effects of physical exhaustion) for three consecutive days. On each trial, the mouse was placed on the drum rotating with 4 rpm along its vertical axis, with its head pointing towards the direction opposite to that of the rod's motion. The mouse had to move forward on the drum in order to avoid falling off. Over a period of 300 s, the rod accelerated to a speed of 40 rpm. Runs in which a mouse did not actively balance on the rod but rather passively clung to it were excluded. After a retention delay of one week, the long-term motor memory of the animals was evaluated during three trials. To probe the relationship between rotarod performance, genotype and age, we fitted these data to a mixed effects model, with genotype (WT, KO), age (6 and 12 months), and day of testing/learning (1, 2, 3, and 4) as fixed effects. As random effects, we had random intercepts and random slopes for subjects (mouse). We report lower-bound (i.e., conservative) p-values calculated using the methodology implemented in R package LMERConvenienceFunctions (Newman et al. 2011).

## Data analysis and statistical tests

Sample sizes were defined using prospective power analysis to assure a power of at least 0.8 to detect an effect at the 5% significance level. For mixed models, we sought to detect a 5% difference for fixed effects. For qPCR analyses,

we aimed to detect an at least twofold difference; for all other tests, we aimed to detect a difference of 20% relative to controls. Power analyses were based on results and variances observed in the previous studies and implemented in R (R Core Team 2015).

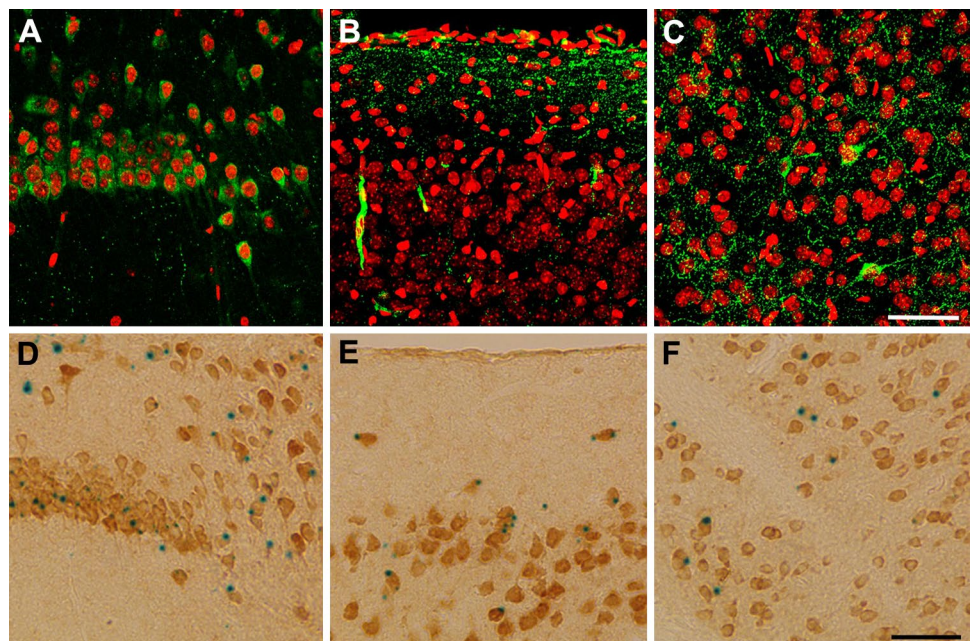
## Results

Initial screening of the central nervous system (CNS) by immunocytochemistry in adult mice showed widespread expression of *Mtss1*, inter alia in the developing cerebral cortex, the hippocampal formation, and the striatum (Fig. 1a–c). The same expression pattern was seen in *Mtss1* heterozygous animals stained for lacZ expressed from the *Mtss1* locus (Figs. 1e, f, 2a, b).

To address the developmental significance of *Mtss1* for cortical histogenesis, we focussed on the cerebellar cortex. This choice was primarily motivated by the fact that cellular interactions during cortical histogenesis are particularly well understood in the cerebellum; and that the key interacting, *Mtss1*-expressing cells in this cortical structure can be readily identified, and selectively and specifically targeted by genetic means.

To assess the effect of *Mtss1* on normal cerebellar function and development, we analyzed motor behavior and cerebellar histogenesis in mice deficient for *Mtss1* (Xia et al. 2010). Of note, animals analyzed here are genetically distinct from those for which similar tests have been described recently (Saarikangas et al. 2015). *Mtss1*<sup>-/-</sup> animals were born at the expected Mendelian frequency and did not show any obviously abnormal behavior or a decreased life

**Fig. 1** *Mtss1* is widely expressed throughout the cerebrum. **a–c** Immunofluorescence staining for *Mtss1* (green) of CA1 (a), cortex (b), and striatum (c) of seven-month-old wild-type mice reveals expression in multiple neuronal subtypes. Propidium iodide was used to stain nuclei (red). Scale bar 50  $\mu$ m. **d–f** Alternatively,  $\beta$ -galactosidase staining to visualize lacZ reporter gene expression in seven-month-old heterozygous *Mtss1*-deficient cells (blue) and counterstaining for NeuN (brown) identifies neurons in the CA1 region (d), cortex (e), and striatum (f) that express *Mtss1*. Scale bar 50  $\mu$ m



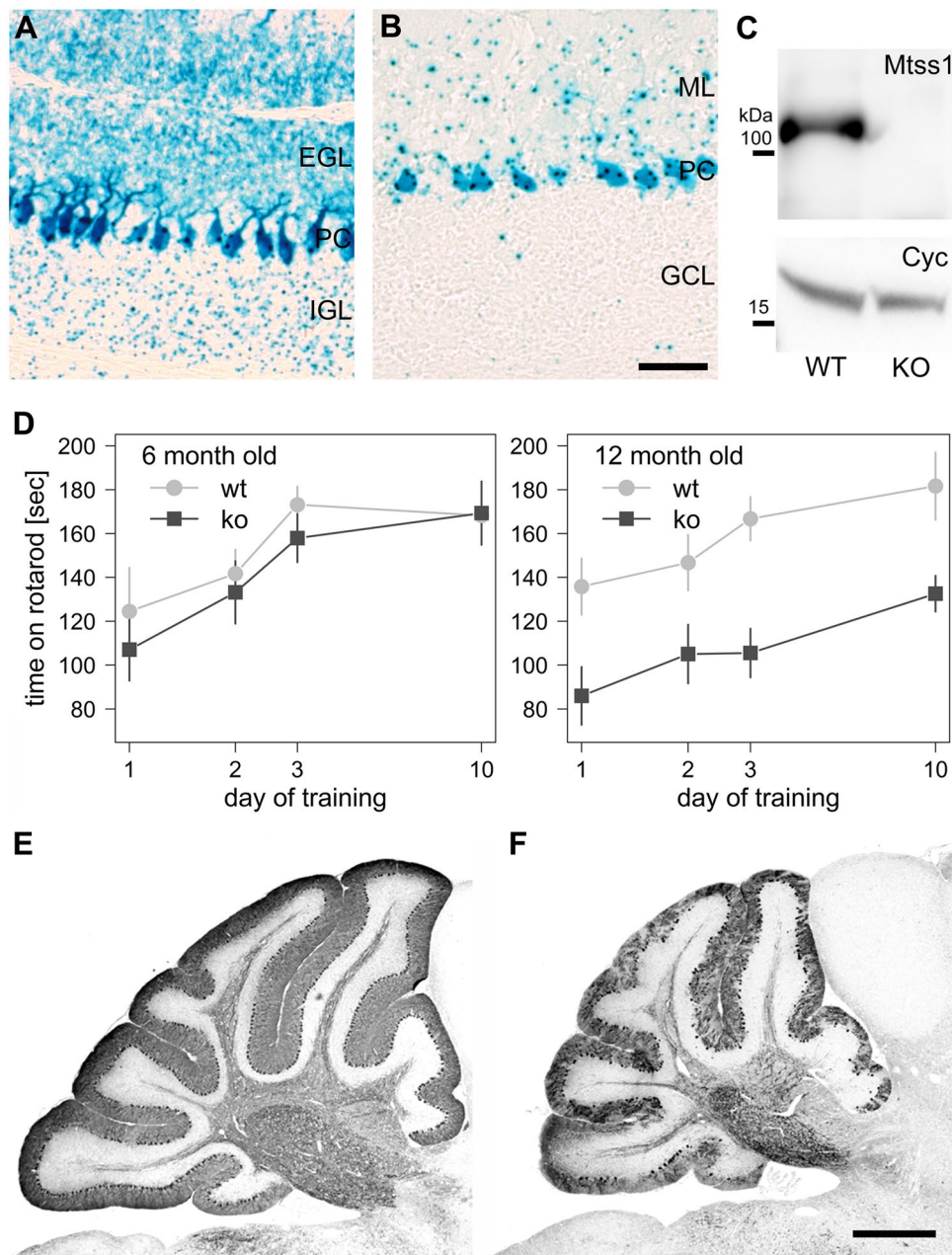


**Fig. 2** Expression of Mtss1 is developmentally regulated and affects rotarod performance and cerebellar size. **a, b** Cerebellar sections of P8 (**a**) and two-month-old  $Mtss1^{-/-}$  mice (**b**) were probed for  $\beta$ -galactosidase activity. Note that at P8 granule cells of the external granular layer (EGL) and the internal granular layer (IGL) as well as Purkinje cells (PCL) are positive for lacZ. In adult  $Mtss1$ -null mice, X-gal staining is still present in Purkinje neurons, but lacking in granule cells. Scale bar 50  $\mu$ m.  $n > 3$  per group. **c** Western blot analysis of Mtss1 proteins in wild-type and  $Mtss1^{-/-}$  cerebellar lysates using an antibody directed to the C-terminal portion (exon 15) of Mtss1. Cyclophilin (Cyc) was used as a loading control.  $n = 2$  independent experiments. **d** At six months of age,  $Mtss1^{-/-}$  (KO;  $n = 15$  mice) and wild-type (WT,  $n = 22$ ) mice show comparable rotarod performances. Both genotypes improve over time in an indistinguishable way ( $F(1, 70)$  for day = 17.95,  $p < 0.001$ ;  $F(2, 70)$  for genotype = 0.33,  $p = 0.567$ ;

$F(2, 70)$  for interaction between day and genotype = 0.49,  $p = 0.486$ ). In contrast, at 12 months of age, the latency to fall of  $Mtss1^{-/-}$  mice ( $n = 15$ ) is considerably worse than that of aged wild-type ( $n = 12$ ) animals ( $F(2, 46) = 16.06$ ,  $p < 0.001$ ), and also that of  $Mtss1^{-/-}$  mice at six months ( $F(1, 68) = 11.65$ ,  $p < 0.001$ ). Note that  $Mtss1^{-/-}$  mice still improved over time, and that the tempo of improvement was comparable to wild-type animals ( $F(1, 46)$  for day = 32.09,  $p < 0.001$ ;  $F(2, 46)$  for interaction between day and genotype = 0.19,  $p = 0.668$ ). Note also that the performance of wild-type is not dependent on age ( $F(1, 88) = 1.47$ ,  $p = 0.229$ ). Error bars indicate 1 SEM. The time axis is on a logarithmic scale. **e, f** Matched parasagittal sections stained for Calbindin reveal a clear-cut reduction in cerebellar size in seven-month-old  $Mtss1$ -null animals (**f**) compared to wild-type littermates (**e**). Scale bar 500  $\mu$ m.  $n = 5$  WT and 4 KO cerebella

span. Cerebellar protein extracts from these mutants probed with an antibody specific to a C-terminal epitope of *Mtss1* showed that these animals were indeed null for this protein (Fig. 2c).

Rotarod testing of the motor skills of *Mtss1*-deficient animals at six months of age did not reveal any differences relative to wild-type littermates (Fig. 2d). At initial testing, the time the animals managed to stay on the rotating rod was the same for *Mtss1*-deficient animals and their wild-type littermates, and both genotypes showed identical improvement (learning) upon retesting on subsequent days ( $p$  for genotype difference = 0.567).

In contrast, when both genotypes were retested at an age of 12 months, *Mtss1*-deficient animals could be clearly distinguished. While the improvement of performance seen on subsequent days was comparable for wild-type and mutant animals, the overall performance of mutants was worse on all days tested ( $p$  for genotype < 0.001). This difference was primarily due to a dramatic reduction in the time-aged mutant animals managed to stay on the rod ( $p$  < 0.001), which contrasted with the rather unchanged performance of wild-type animals at six and 12 months of age ( $p$  = 0.229).

### ***Mtss1* ablation severely impairs Purkinje cell survival and morphology**

To search for the pathology underpinning this behavioral phenotype, we initially compared cerebellar sizes of wild-type and *Mtss1*-deficient animals. Overall, cerebellar size of *Mtss1*-deficient animals was clearly reduced as compared to wild-type littermates (Fig. 2e, f). When we measured the length of the Purkinje cell layer in mid-sagittal sections, this size indicator was reduced by 19% in knockout animals ( $n$  = 5 WT and 4 KO animals;  $p$  = 0.043;  $t$  test). These sections also revealed widespread and scattered Purkinje cell loss throughout the cerebellar cortex, indicated by a patchy and irregular staining for Calbindin. We could not observe any anterior–posterior or mediolateral pattern of Purkinje cell demise. To delineate the time course of these changes, we analyzed sections of animals aged between eight days and 12 months (Fig. 3). The most conspicuous finding was a progressive loss of Purkinje cells over age. While no differences in the density of Purkinje cells were visible at P8, P21, and two months of age, massive gaps in the Purkinje cell layer were visible in cerebella obtained from seven- and 12-month-old animals (Fig. 3a, b). At higher magnification, besides the overt loss of Purkinje neurons, variability in their staining intensity and a somewhat disordered arrangement of their dendrites became apparent. Specifically, major dendritic branches in *Mtss1*<sup>-/-</sup> animals are often oriented towards the granule cell layer, rather than towards the meningeal surface, as is the rule in wild-type mice (a phenotype somewhat reminiscent of the weeping willow

dendrites described by Altman and Anderson (1972); compare Fig. 4a, b. In 36 wild-type cells, downward orientation of main dendrites occurred only twice. In contrast, 24 such misoriented dendrites were observed in 33 Purkinje cells deficient for *Mtss1* ( $p$  =  $1.58 \times 10^{-9}$ ; G-test with William's correction). A conspicuous feature visible in major dendrites of *Mtss1*<sup>-/-</sup> animals was oval areas, typically measuring some 4–6  $\mu$ m in diameter, devoid of Calbindin signal. Careful inspection of serial optical sections strongly suggested that these structures resulted from a local thinning or indentation of Purkinje cell dendrites. Similar to the major dendritic branches, tertiary branchlets of Purkinje cell dendrites in *Mtss1* animals showed an abnormal orientation, often pointing downward (i.e., towards the granule cell layer, but without entering it). At first glance, they also appeared thinner and less straight than those in wild-type animals. Analysis at still higher resolution (Fig. 4c–f) confirmed this impression and further revealed that the density of tertiary branchlet spines was lower in *Mtss1*-deficient animals as compared to controls (protrusions/ $\mu$ m of dendrite: *Mtss1*<sup>+/+</sup>,  $2.6 \pm 0.14$ , *Mtss1*<sup>-/-</sup>,  $1.7 \pm 0.09$ ,  $p$  = 0.0003,  $t$  test,  $n$  = 3 animals per genotype with 12–13 cells per animal).

The development of Purkinje and granule cells is tightly interconnected. Thus, the above findings in mice globally null for *Mtss1* do not allow to dissect the primary cellular site(s) of action of this protein during normal Purkinje cell development. To address this issue, we bred *Mtss1*-KO animals with mice expressing the cre recombinase either under control of the granule cell-specific *Atoh1* (*Math1*) promoter (Ben-Arie et al. 1997), or the Purkinje cell-specific *Pcp2* (*L7*) promoter (Oberdick et al. 1990). This allowed re-expression of *Mtss1*, on an *Mtss1*-deficient background, specifically in granule cells and their precursors or postmitotic, postmigratory Purkinje cells, respectively. We visualized the wild-type status of individual cells by staining for  $\beta$ -galactosidase, which is expressed only in *Mtss1*-null cells, and we used western blotting to assess expression strength of *Mtss1* (Supplementary Fig. 1).

In *Mtss1*-null animals in which *Mtss1* was selectively re-expressed in Purkinje cells, cell-free gaps indicative of Purkinje cell loss were no longer detectable, and consequently, overall dendritic density was also higher in these animals than in *Mtss1*-null mice. However, the structure of Purkinje cell dendrites was still abnormal, with kinks in major dendritic stems and downward oriented tertiary branchlets reminiscent of the situation in mice globally null for *Mtss1* (Fig. 4g). Conversely, in mutant animals in which expression of this gene was selectively restored in granule cells (Fig. 4h), Purkinje cell gaps were the most prominent finding. Further, Purkinje cell dendrites were stunted and disfigured, as described above following the global knockout of this gene (Fig. 4d).



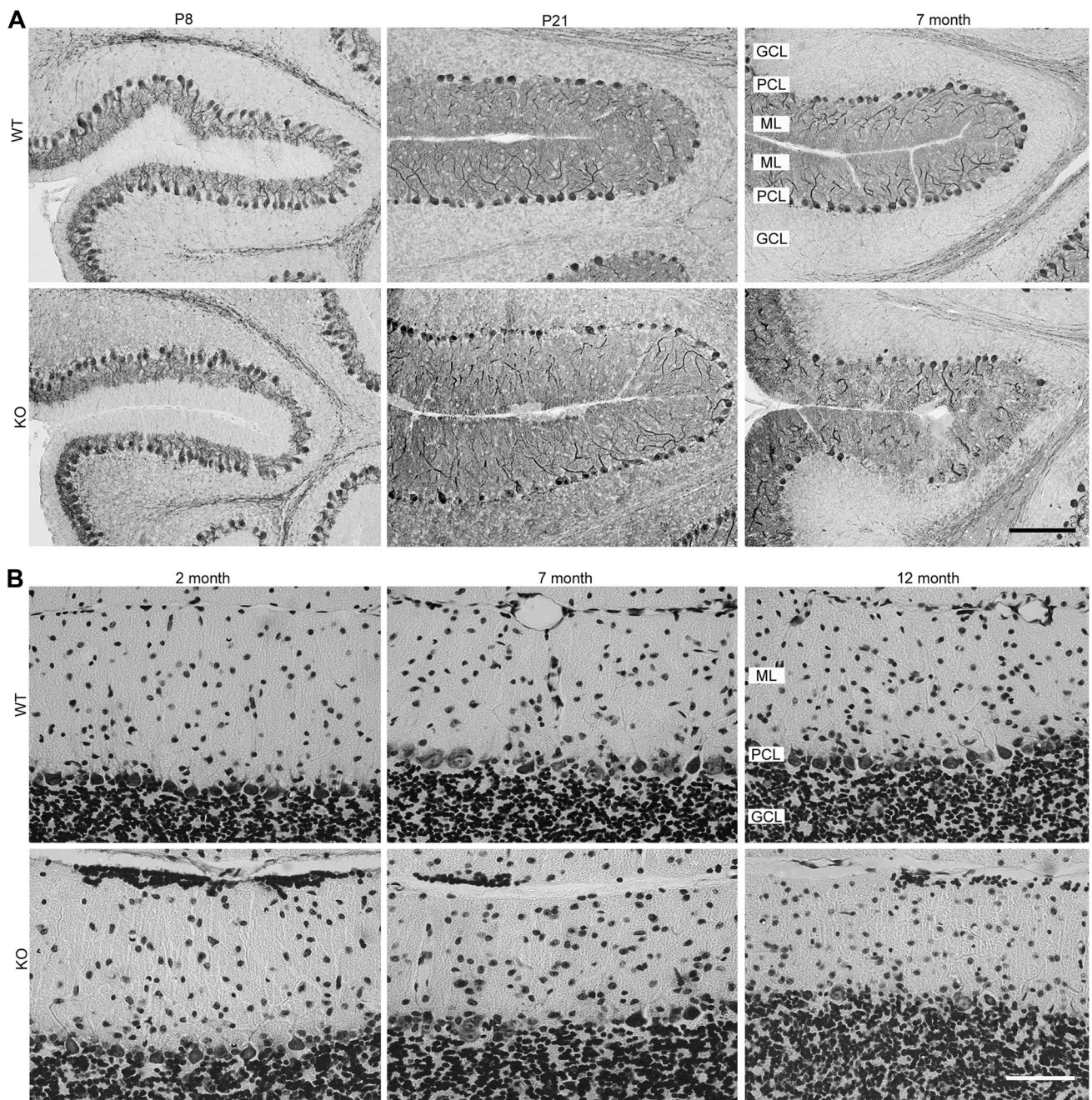


**Fig. 3** Ablation of *Mtss1* causes impaired survival of Purkinje neurons. **a** Immunocytochemical staining for Calbindin shows a regular layer of Purkinje cells in wild-type (WT) and mutant mice (KO) at eight and 21 days of age, but multiple regions devoid of Purkinje cells in seven-month-old animals. Scale bar 250  $\mu\text{m}$ .  $n=5$  per group. **b**

This observation is confirmed in Nissl-stained sections, which appear indistinguishable in two-month-old animals, but show massive gaps in the Purkinje cell layer in seven- and 12-month-old animals. Scale bar 50  $\mu\text{m}$ .  $n=5$  per group

Another difference between Purkinje cells in WT and *Mtss1*<sup>-/-</sup> animals was the presence, in the latter, of multiple swellings in the axons (axon collaterals) that form the subganglionic plexus. These appeared as bead-like, roundish structures with a diameter of around 5–6  $\mu\text{m}$ , clearly larger than axonal swellings characteristic for the subganglionic

plexus in wild-type mice (2–3  $\mu\text{m}$  in diameter). Consistently, Purkinje cell axon terminals identified by staining for Calbindin surrounding deep nuclear neurons were also larger in *Mtss1*-deficient animals as compared to controls (Fig. 5a, b). Quantitative analysis showed that this was due to a gain of large-diameter terminals, and a compensatory

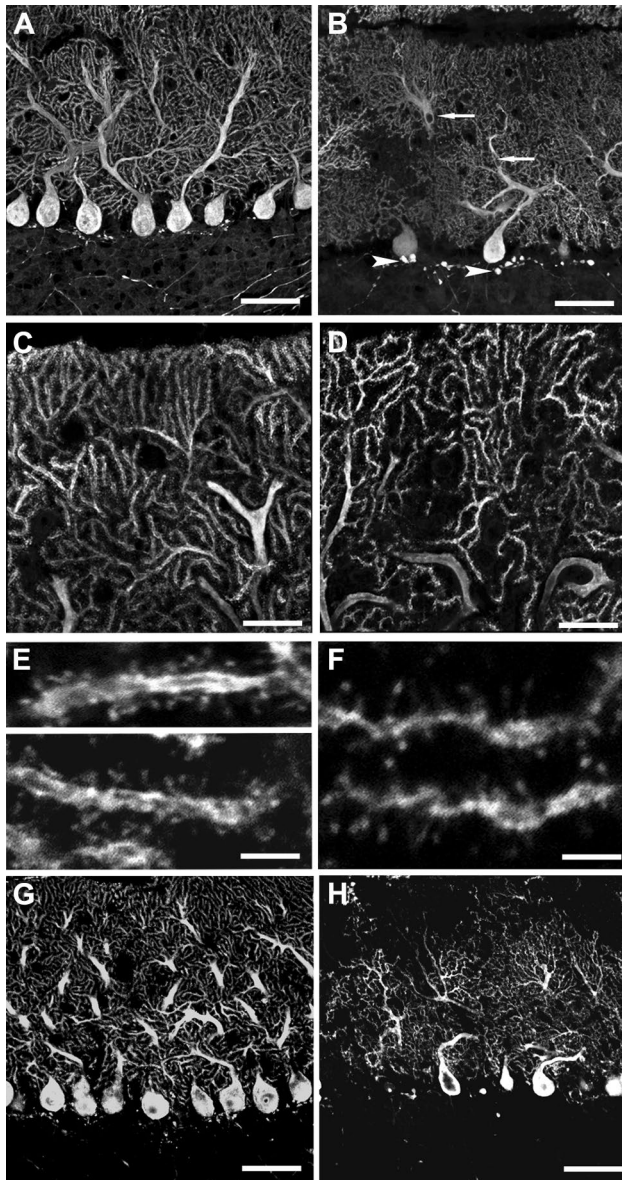


**Fig. 4** Altered Purkinje cell dendritic morphology in *Mtss1*<sup>-/-</sup> mice. **a, b** Commensurate with Purkinje cell loss in aged *Mtss1*<sup>-/-</sup> animals, parts of the molecular layer were devoid of Purkinje cell dendrites, giving it an overall patchy appearance in sections stained for Calbindin (**b**; **a** shows an age-matched wild-type). Note also the somewhat kinky course of main dendritic branches in the mutant, and the presence of ovoid structures devoid of immunosignal (*arrows* in **b**). Finally, note that axonal swellings in the subganglionic plexus are considerably larger in seven-month-old *Mtss1*<sup>-/-</sup> animals than in controls (*arrowheads* in **b**). *Scale bar* 50  $\mu$ m. *n*=4. **c, d** Higher power views of representative areas of the molecular layer again show differences in dendritic density between wild-type (**c**) and *Mtss1*<sup>-/-</sup> mice (**d**). *Scale bar* 20  $\mu$ m. **e, f** At still higher magnification, spine density appears noticeably reduced in mutant mice. *Scale bar* 2  $\mu$ m. **g, h** Purkinje cell dendritic morphology approaches that seen in wild-type cells following re-expression of *Mtss1* in these cells (**g**). In contrast, Purkinje cell dendrites are still dysmorphic if re-expression of *Mtss1* occurs selectively in granule cells (**h**). Purkinje cells were identified by immunostaining for Calbindin. *Scale bar* 50  $\mu$ m, *n*=5

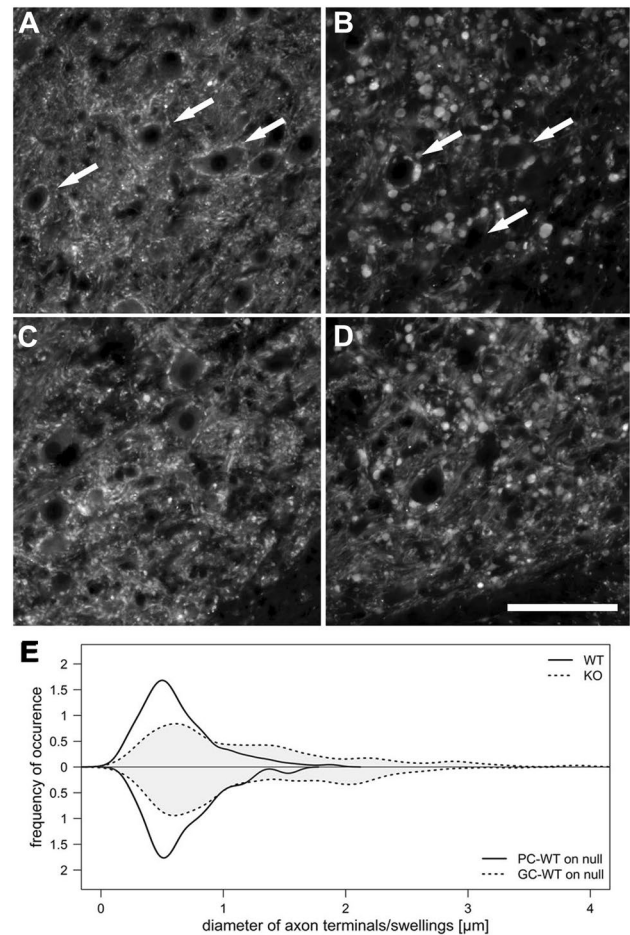


**Fig. 5** *Mtss1* ablation causes increased size of Purkinje cell axon terminals. **a, b** Calbindin-immunoreactive Purkinje cell axon terminals surrounding somata (*arrows*) of neurons in the dentate nucleus of age-matched (seven-month old) wild-type (**a**) and global *Mtss1*<sup>-/-</sup> mice (**b**). *n*=3 per group. *Scale bar* 250  $\mu$ m. **c, d** Terminals of Purkinje cell axons of mice in which Purkinje cells were reverted to wild-type status (**c**) and of mice which re-expressed *Mtss1* in granule cells (**d**). *n*=3–4 per group. *Scale bar* 250  $\mu$ m. **e** Purkinje cell axon terminals in global *Mtss1*<sup>-/-</sup> mice and animals in which granule cells were reverted to wild-type status are skewed towards larger sizes relative to that seen in wild-type mice or in animals with Purkinje cell-specific re-expression of *Mtss1*. *n*=3–4 mice per group, *n*=328 terminals for WT, 211 for KO, 215 for animals in which granule cells were wild-type on a null background and 162 terminals for animals with wild-type Purkinje cells on a null background

reduction of the fraction of smaller terminals, which, however, were still present in *Mtss1*-deficient animals (Fig. 5e). The median size of terminals in *Mtss1*<sup>-/-</sup> mice was 0.93 vs 0.56  $\mu$ m in wild-type animals. More than 15% of all terminals in *Mtss1*<sup>-/-</sup> animals were larger than the largest ones observed in wild-type mice (Fig. 5e, *p*<0.001 by Kolmogorov–Smirnov test for equality of distributions). Re-expression of *Mtss1* in Purkinje cells fully reverted this axonal/presynaptic phenotype (Fig. 5c; WT vs *Mtss1*-positive Purkinje cells on a null background, *p*>0.3). In contrast,

re-expression in granule cells had no effect on the aberrant presynaptic structure of Purkinje cells (Fig. 5d,  $p < 0.001$  for comparison with WT or *Mtss1*-positive Purkinje cells on a null background; and  $p > 0.5$  for KO vs *Mtss1*-positive granule cells on a null background).

### *Mtss1* deficiency causes displaced and morphologically altered granule cells

Besides Purkinje neurons, granule cell development was also affected in *Mtss1*-deficient animals. While no obvious differences were visible at P8, multiple sub-meningeal granule cell ectopias were observed from P21 onward

(Fig. 6a). These were more frequent in the posterior lobes of the cerebellum and typically consisted of small, flat clusters of cells that stained strongly for NeuN, which, within the cerebellar cortex, is a specific marker for postmitotic and postmigratory granule cells (Weyer and Schilling 2003).

As documented in Fig. 6d, granule cell ectopias persisted in cerebella of *Mtss1*-null mice in which *Mtss1* was re-expressed in Purkinje cells. While ectopias persisted also after restoration of *Mtss1* expression in granule cells, they were considerably smaller in these animals than those seen in animals in which granule cells and their precursors were null for *Mtss1* (Fig. 6e).

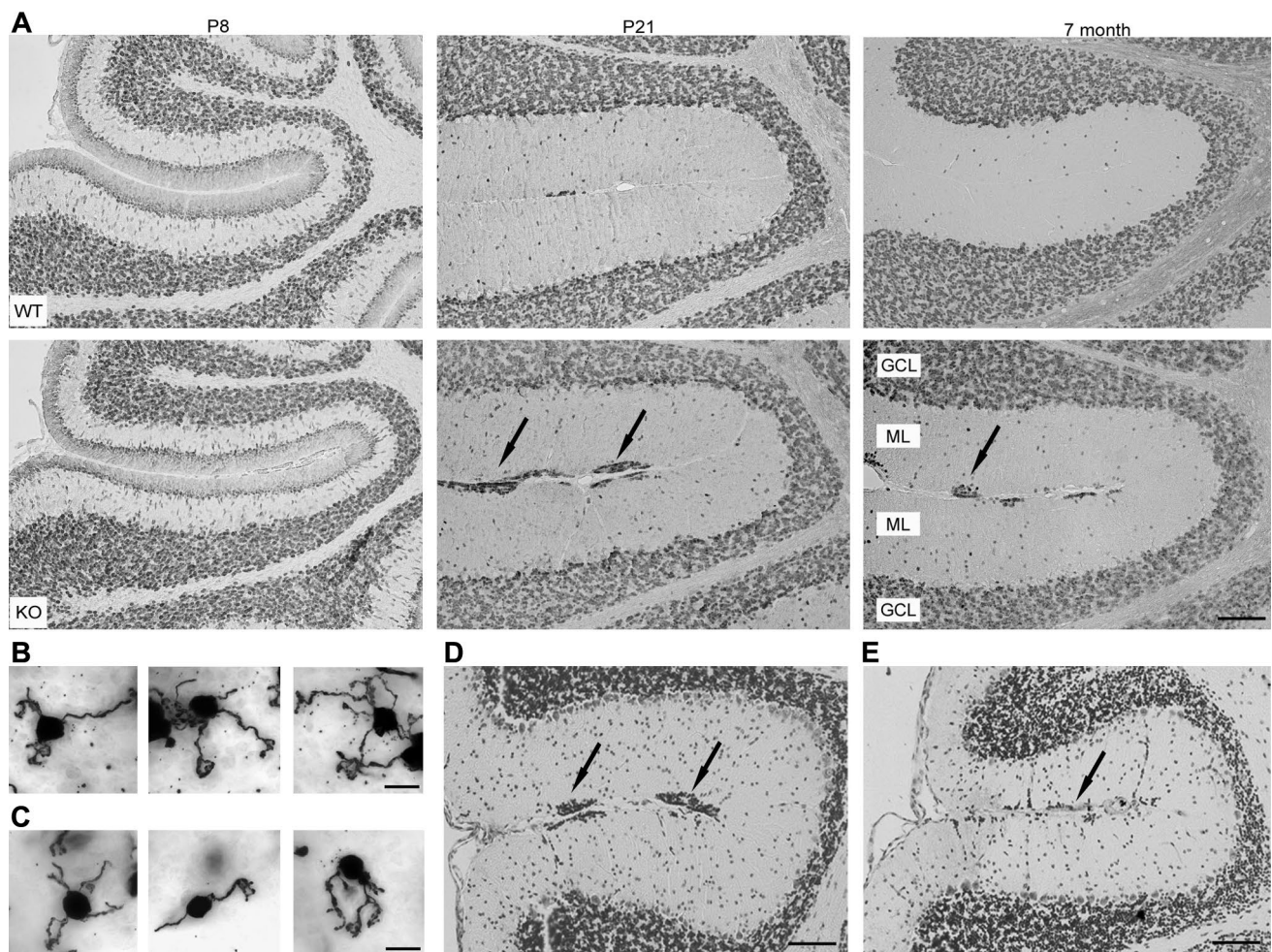


**Fig. 6** Loss of *Mtss1* leads to displaced and morphologically altered cerebellar granule neurons. **a** At P8, the localization of postmitotic NeuN-positive granule cells is indistinguishable in wild-type (WT upper row) and *Mtss1*-deficient animals (KO lower row). At P21, when the external granular layer has just vanished, as well as in seven-month-old animals, *Mtss1* KO cerebella show ectopically clustered granule cells in the molecular layer (arrows). Note that the amount of postmitotic granule cells dispersed in the molecular layer of *Mtss1*<sup>-/-</sup> cerebella seems to be increased in all ages investigated.

Scale bar 150  $\mu$ m.  $n = 4-6$  per age. **b, c** Representative examples of Golgi-stained granule cells of *Mtss1* wild-type (**b**) and mutant cerebella (**c**). Scale bar 10  $\mu$ m.  $n = 3$  per group. **d, e** Nissl staining documents the persistence of granule cell ectopias following the reconstitution of *Mtss1* expression in Purkinje cells (**d**). Following re-expression of *Mtss1* in granule cells (and their precursors), ectopias are largely gone, although minor ones can still be detected (**e**). Scale bar 150  $\mu$ m.  $n = 5$  animals aged 6–7 month

To get a quantitative perspective on these ectopias, we measured, in matched sagittal sections from the vermis cerebelli, the size of sub-meningeal granule cell clusters. Previous investigations have shown that such ectopias may occur, if rarely, in wild-type C57Bl/6 mice. If so, they are restricted to lobules VIII and IX, where they impressed as cellular bridges between the granule layers of these lobules these lobules (van Dine et al. 2015).

Therefore, we carefully screened wild-type littermates of our *Mtss1*-deficient animals for granule cell ectopias. In keeping with the above reports, we did not observe ectopias in more than 20 animals screened. In contrast, in *Mtss1*-deficient animals, ectopias were found scattered all along the anterior–posterior axis. They occurred at about the same frequency (range=17–32 per section) as in mice in which Purkinje cells were reverted to a wild-type status (range=20–23). Numbers of ectopias were lower in *Mtss1*-null animals in which *Mtss1* was reverted to a wild-type status in granule cell precursors (range 9–16). Further, in these latter animals, remaining ectopias were restricted to the posterior cerebellum. This difference became even more obvious when we assessed the size of these ectopias (taking their area in sagittal sections as a proxy of total size): While ectopias were of about the same size in *Mtss1*-null animals and *Mtss1*-null animals with re-expression of *Mtss1* in Purkinje cells (17,906  $\pm$  961  $\mu\text{m}^2$  vs 20,334  $\pm$  4137  $\mu\text{m}^2$ ;  $p=0.664$ ; Anova for genotype effect, followed by Tukey's post hoc test), they were considerably smaller in animals in which *Mtss1* expression was restored to granule cell precursors (5052  $\pm$  402  $\mu\text{m}^2$ ;  $p=0.001$  when compared to *Mtss1*-null mice). Thus, *Mtss1* deficiency results in granule cell ectopias that are not appreciably reduced by selective re-expression of *Mtss1* in Purkinje cells, but are largely reduced following the re-expression in granule cell

precursors. Persistent granule cell ectopias in the latter animals are located in posterior cerebellum, where the *Atoh1* (*Math1*) promoter used to bring about *Mtss1* reconstitution to granule cell precursors is known to be not fully effective (Machold and Fishell 2005; Pan et al. 2009; see also "Discussion").

Further, as compared to wild-type littermates, increased numbers of single postmitotic granule cells were found in the molecular layer of adult *Mtss1*-deficient animals (Fig. 6a). A comparison of Golgi-stained cells present in the granule cell layer of adult *Mtss1*<sup>-/-</sup> and wild-type mice revealed multiple anomalies including shortened or missing dendrites or bulged soma (Fig. 6b, c) in *Mtss1*-deficient granule neurons.

To investigate whether ectopias were caused by altered granule cell precursor proliferation, we stained early postnatal cerebellar sections with the proliferation marker PCNA. Comparison of the genotypes did not reveal any differences between cerebella of wild-type and *Mtss1*<sup>-/-</sup> animals (Fig. 7a, b). Further, cells isolated from eight-day-old postnatal cerebellar anlagen of wild-type and *Mtss1*<sup>-/-</sup> animals showed equal numbers of cells incorporating BrdU. This series of experiments also revealed that *Mtss1*-deficient cells showed the same sensitivity towards the granule cell mitogen, sonic hedgehog as wild-type cells (Fig. 7c).

#### Developmental expression and cellular localization of *Mtss1* isoforms in the cerebellum

Any mechanistic interpretation of the morphological deficits outlined above needs to consider that two splice variants of *Mtss1* are expressed in the CNS, and specifically during cerebellar development (Glassmann et al. 2007). To



**Fig. 7** *Mtss1* is dispensable for granule cell proliferation. **a, b** PCNA staining of P8 *Mtss1*<sup>+/+</sup> mouse cerebella (**a**) shows no histological alterations compared with *Mtss1*<sup>-/-</sup> mouse tissue (**b**). Scale bar 150  $\mu\text{m}$ .  $n=3$  per group. **c** Ablation of *Mtss1* does not influence the proliferation of primary granule neurons as measured by the percentage of cells that incorporated BrdU (WT vs KO,  $p=0.969$ ). Shh leads to a massive increase of the fraction of cells that incorporated

BrdU both in *Mtss1*<sup>+/+</sup> and *Mtss1*<sup>-/-</sup> cultures (for both, Shh vs no treatment,  $p \leq 0.001$ ). Yet as for untreated cells, numbers of BrdU-positive cells in wild-type and *Mtss1*-deficient cultures could not be distinguished ( $p=0.714$ ) following Shh treatment. Error bars are SEM.  $n=2$  independent experiments with 625–1211 cells scored per genotype and condition

date, the function of the CNS-specific isoform of Mtss1 is still elusive.

To address this issue, we sought to obtain a quantitative estimate of Mtss1 splice variant expression during cerebellar development and to assess the (sub-) cellular location of the respective protein products. Expression of Mtss1 mRNA is stronger at P8 as compared to P0 or adults. This is true for both the exon 12 and exon 12a isoform (Fig. 8a). Overall, expression of the exon 12a variant is considerably stronger than that of the exon 12 variant (about 12–17 fold), with the biggest differences seen in adults (~120-day-old animals). However, age-dependent changes in relative expression levels of these two exons were rather moderate.

To clarify whether both Mtss1 isoforms are expressed by the same cell or whether they are differentially expressed in distinct cell types, we used antibodies specific for Mtss1 isoforms comprising either exon 12 or 12a. Staining of cerebellar sections of P8 mice with these antibodies revealed that both Mtss1 isoforms were expressed in Purkinje neurons and in granule cells, both in the EGL and the IGL. In two-month-old animals, immunoreactivity for Mtss1 was no longer visible in granule cells (Fig. 8b). In Purkinje neurons, the subcellular localization of the immunosignal was strikingly different for the two isoforms. Staining for both splice variants resulted in an outlining of entire Purkinje cells, including their dendritic trees and also their axons, which can readily be identified passing the granule cell layer. In contrast, in adult Purkinje cells, the exon 12 variant of Mtss1 localizes to the nucleus, whereas that comprising exon 12a was excluded from it. Finally, it seems appropriate to note that these antibodies also permitted us to verify that Mtss1-deficient animals were indeed devoid of both Mtss1 isoforms (Fig. 8c).

### Splice variant-specific effects of Mtss1 on granule cell development

To further probe how Mtss1 might affect granule cell development, and particularly to assess potentially specific effects of its splice isoforms, we next studied cerebellar granule cell development *in vitro*. As in the intact cerebellum, expression of the Mtss1-exon 12a isoform is considerably stronger than that of the exon 12 variant over ten days of cultivation (Fig. 8a). Of note, the transcription level of the Mtss1 isoform comprising exon 12 is constantly reduced from DIV 1 to DIV 10. In contrast, the amount of mRNA encoding the exon 12a variant increases until DIV 3 but then drops during further maturation.

Next, we compared the motility of granule cells in primary cultures prepared from wild-type and Mtss1-deficient mice. After seeding, cells were allowed to adhere to the substratum for four hours; they were then tracked for five hours. Figure 9b shows the (time- and ensemble-averaged)

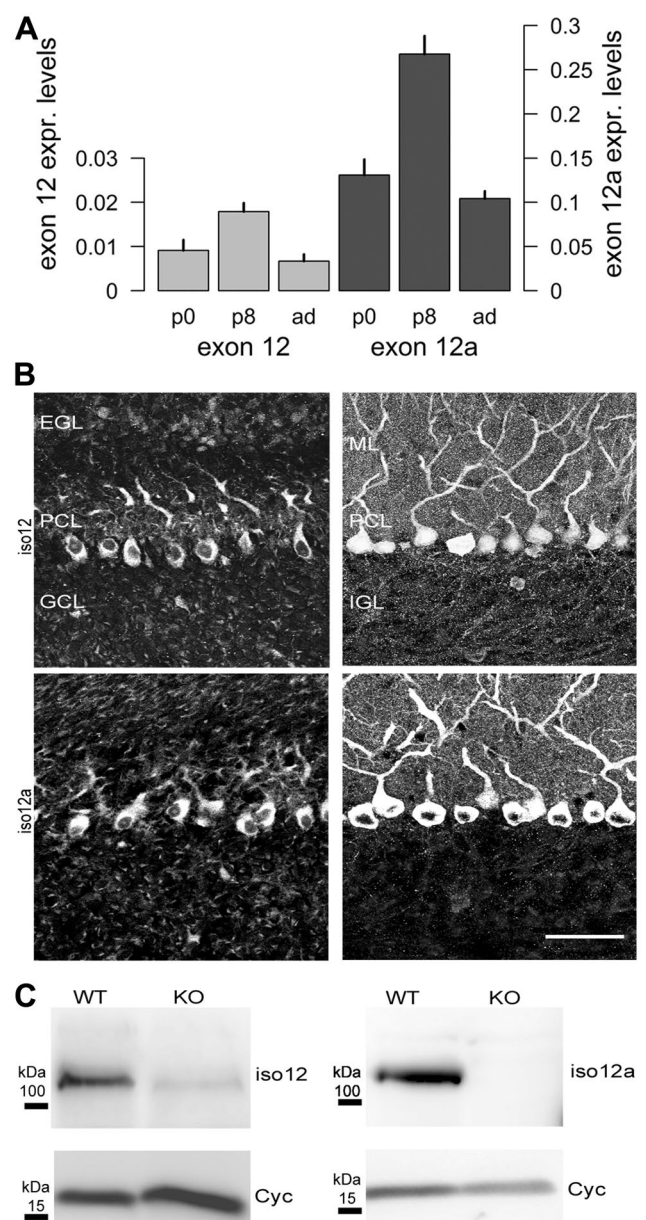
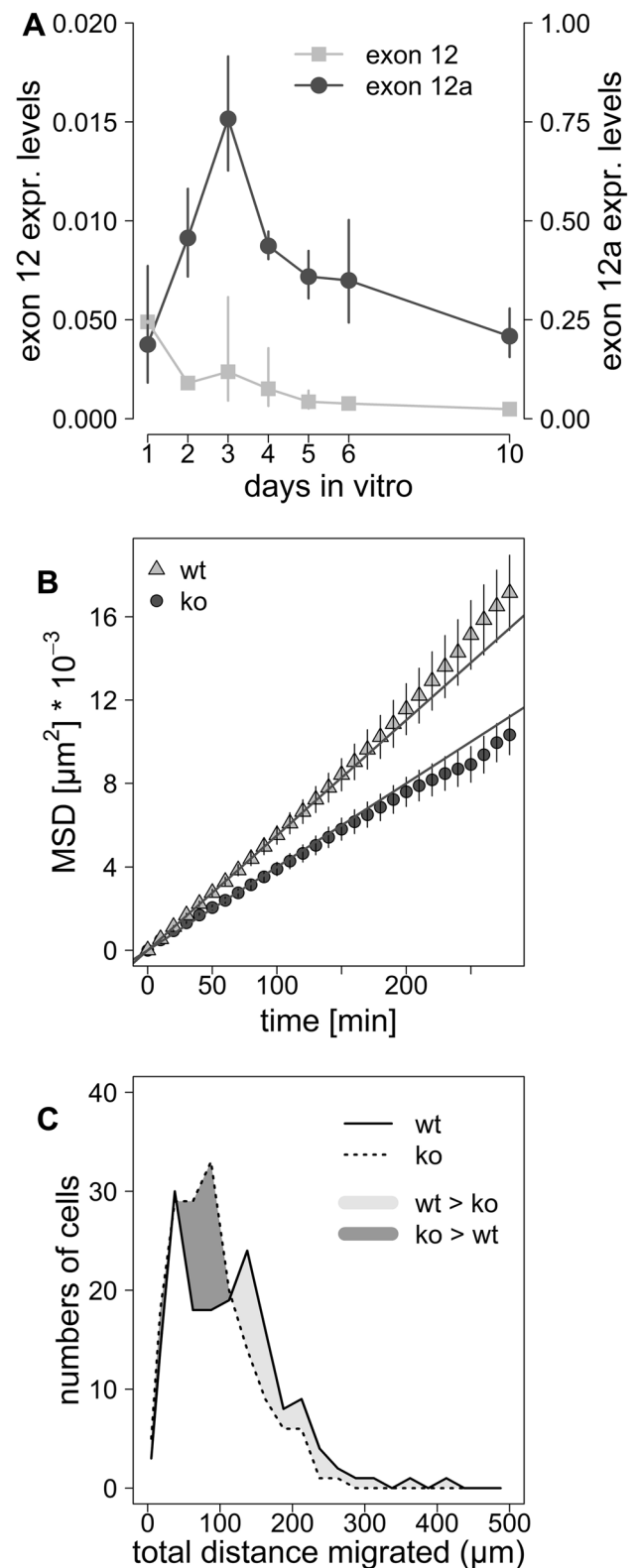


**Fig. 8** Mtss1 isoforms are differentially expressed in maturing cerebellum. **a** qPCR analysis of Mtss1 splice isoforms comprising exon 12 or exon 12a in Mtss1 wild-type animals at different developmental stages. Note the fivefold difference of scales for exon 12 and exon 12a. Expression levels are relative to that of GAPDH.  $n=4$  per age. Error bars = 1 SEM. **b** Cerebellar sections of P8 and two-month-old WT mice were stained with antibodies specific to Mtss1 splice isoforms harboring exon 12 (iso12) or exon 12a (iso12a). At P8, both isoforms show comparable cell type-specific and subcellular localization. In adult cerebellum, granule cells cease to express Mtss1, whereas in Purkinje cells Mtss1 protein is still detectable. In mature, Purkinje cells Mtss1-exon 12 localizes to the nucleus but Mtss1-exon 12a does not. EGL: external granular layer, PCL: Purkinje cell layer, IGL: internal granular layer, ML: molecular layer, GCL: granule cell layer. Scale bar 50  $\mu\text{m}$ .  $n=3$  animals per age. **c** Western blot analysis of Mtss1 wild-type (WT) and Mtss1-deficient (KO) cerebellar lysates probed with antibodies directed to Mtss1-exon 12 or -exon 12a displaying complete loss of both isoforms in Mtss1<sup>-/-</sup> brain.  $n=2$  independent experiments

**Fig. 9** Expression of *Mtss1* isoforms and mobility of cultured granule cells. **a** qPCR analysis of *Mtss1* splice isoforms comprising exon 12 or exon 12a in wild-type primary granule cells at different developmental stages. Expression levels are relative to that of GAPDH. Note the fivefold scale difference of scales for exon 12 and exon 12a. DIV: days in vitro. Error bars are SEM of two independent experiments. **b** Mean square displacement (MSD) analysis of the trajectories of *Mtss1*<sup>+/+</sup> and *Mtss1*<sup>-/-</sup> granule cells (169 and 172 cells, respectively; 28 time points each). When these data were fitted to a power functions of the form  $MSD \sim K \times \text{time}^{\alpha}$ , the directional persistence-associated parameter alpha differed for wild-type and KO cells ( $1.011 \pm 0.004$  vs  $0.942 \pm 0.009$ ;  $p = 1.16 \times 10^{-8}$ ), and both differed from unity ( $p = 0.038$  and  $1.19 \times 10^{-6}$ , respectively). Fits expected for  $\alpha = 1$  are shown as straight lines. The speed-related parameter *K* is not significantly different for wild-type and *Mtss1*-null cells ( $52.76 \pm 1.06$  vs  $51.40 \pm 2.08$ ;  $p = 0.667$ ). Error bars are SEMs. **c** Distributions of absolute distances covered by wild-type (solid line) and *Mtss1* KO cells (dotted line) over 280 min in vitro. Dark-shaded areas indicate distances for which *Mtss1* KO cells outnumber wild-type cells, and lightly shaded areas distances for which wild-type cells prevail

mean square displacement (MSD) values obtained from these tracks. These MSD curves provide information on at least two salient issues. First, they allow assessing average cell motility (speed), which may be derived from the slope of the fitted straight lines. Second, they inform us about directional persistence of migrating cells. This latter information is represented in the deviations of data points from the straight line fit (for formal details, see below). Thus, MSD values of wild-type and *Mtss1*-deficient cells seem to deviate systematically from what would be predicted assuming purely random (Brownian, diffusive) motion; the latter prediction is indicated by the straight line fits in Fig. 9b. Intriguingly, this deviation differs, in direction, for wild-type and *Mtss1*<sup>-/-</sup> cells.

To test this, we next fitted the data to power functions of the form  $MSD \sim K \times \text{time}^{\alpha}$  (Metzler and Klafter 2000; Ruthardt et al. 2011). In this model, a value of one for alpha is indicative for a purely diffusive (Brownian) mode of locomotion; values smaller than one indicate hindered (corralled) locomotion, and values between 1 and 2 indicate superdiffusion (or directed movement). *K* is a parameter composed of a constant characteristic for dimensionality of the observations (4 in the present case, as we observed migration in 2-dimensional space), and the “diffusion constant.” For cell movement, this latter may more appropriately called “random motility coefficient” (Dickinson and Tranquillo 1993). Comparison of the parameters of these fits (legend to Fig. 9) for WT and *Mtss1*-deficient cells reveals several facts. First, *K* appears to be about the same for both genotypes ( $p = 0.667$  by two-sided *t* test). In contrast, alpha is different for the two genotypes ( $p = 1.15 \times 10^{-8}$  by two-sided *t* test). Alpha calculated for wild-types is slightly larger than unity. While the difference may appear subtle, it is clearly significant ( $p = 0.038$  by two-sided



*t* test). In contrast, alpha for *Mtss1*-null cells is clearly smaller than one ( $p = 1.19 \times 10^{-6}$ ). As alpha enters the model as an exponent, this indicates a major difference in overall motility, i.e., while motility of wild-type cells shows

some minor degree of directional persistence even in the unstructured *in vitro* environment, that of *Mtss1*<sup>-/-</sup> cells appears hindered, or corralled. This difference in motility is also reflected in the absolute distance covered by the cells during the observed period. Most *Mtss1*-deficient cells were found up to 100–150  $\mu\text{m}$  from their starting point after 280 min of migration (Fig. 9c). There was a clear shift in the distribution of the distances covered towards larger values for wild-type cells. If we define cells that had moved away from their starting point less than 10  $\mu\text{m}$  (i.e., roughly twice the diameter of a typical granule cell soma) as “immobile,” we found that some 1.8 and 2.9% of all cells (3 and 5 cells, in absolute numbers) fell into this category for wild-type and *Mtss1*-deficient cells, respectively.

During migration, granule cells also elaborate their axons and dendrites. To directly probe potential effects of *Mtss1* variants on granule cell neuritogenesis, we compared neurite formation in cultured granule cells from *Mtss1*-deficient animals in which we re-expressed, via viral transduction, *Mtss1*-exon 12, or exon 12a. We verified efficient expression in transduced cells by western blotting (Fig. 10a). While only weak expression of virally transduced *Mtss1* was visible after 6 DIV, a strong signal was obtained at DIV 10 (Fig. 10a).

When we compared neurite densities in these cultures (Fig. 10b), we observed that following viral transduction of *Mtss1*-null cells with the exon 12a comprising isoform of *Mtss1* neurite densities reached wild-type levels at DIV 6, and even surpassed these after 10 DIV. In contrast, expression of the exon 12-comprising isoform of *Mtss1* in *Mtss1*-null granule cells did not lead to a detectable effect on neurite densities after 6 DIV, and caused only a minor increase after 10 DIV. These effects were robust and highly significant ( $p$  at least  $<0.01$ , Fig. 10c).

## Discussion

### *Mtss1* affects dendritic and axonal development

In the cerebellum, *Mtss1*-deficiency results in malformed dendrites and axons, notably of Purkinje and granule cells. Yet these cells not only both express *Mtss1*, but also impinge on each other's morphogenesis (see, e.g., Schilling et al. 1991a; Baptista et al. 1994). To unambiguously identify the cellular site(s) of action responsible for the observed phenotype, we therefore re-expressed, on a global *Mtss1*-null background, *Mtss1* specifically and selectively in Purkinje or granule cells. As Purkinje cell dendritic abnormalities characteristic for *Mtss1*-null mice persist if this gene is re-expressed selectively in granule cells (and their precursors), it follows that *Mtss1* expression in Purkinje cells proper is critical for their dendritogenesis.

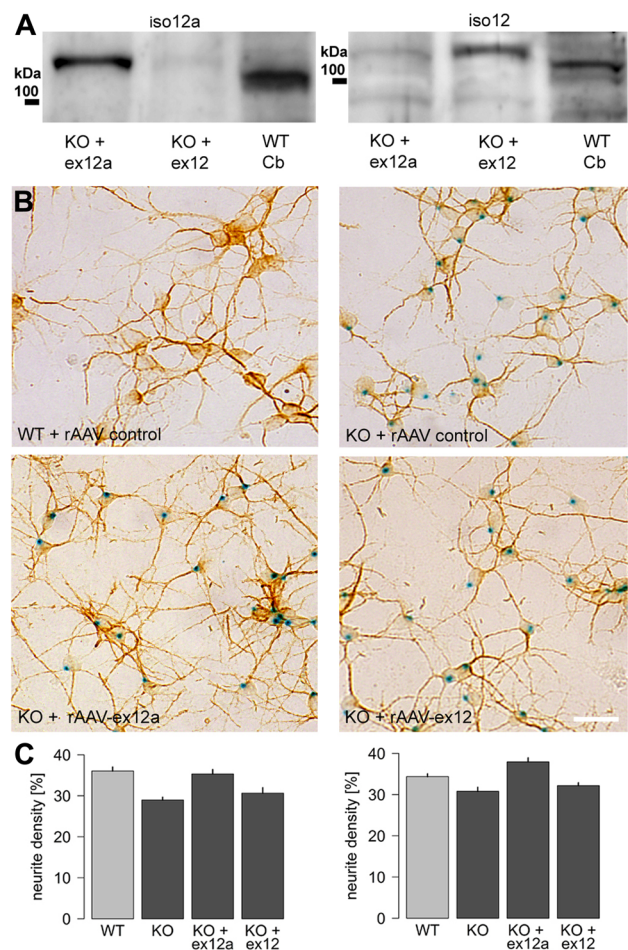


**Fig. 10** *Mtss1*-deficient granule cells display reduced neurite development that can be rescued by expression of *Mtss1*-exon 12a. **a** Western blot analysis of primary cerebellar granule cells transduced with rAAV-exon 12a and rAAV-exon 12. The size difference of *Mtss1* bands of transduced primary neurons compared to wild-type cerebellar lysate is caused by the Strep-tag added to the N-terminus of the transduced proteins. Cyclophilin (Cyc) was used as a loading control. Results are representative data of two independent experiments. **b** Representative images of X-gal and Map2-stained primary cerebellar granule cells after six days *in vitro*. *Mtss1*<sup>-/-</sup> neurons have less neurites compared to granule cells derived from *Mtss1*<sup>+/+</sup> littermates. Upon rAAV-mediated expression of *Mtss1*, phenotypical rescue can be achieved only by *Mtss1*-exon 12a. Scale bar 15  $\mu\text{m}$ . **c** Quantitative analysis of neurite density following expression of either exon 12 or exon 12a variant of *Mtss1*. Neurite density in *Mtss1*-deficient (KO) cells is clearly lower than in wild-type (WT) cells (at DIV 6 and DIV 10,  $p < 0.001$ ). Following expression of *Mtss1*-exon 12a in KO-granule cells, neurite density increases and is no longer distinguishable (at DIV 6,  $p = 0.877$ ) or even exceeds that in wild-type cells (at DIV 10,  $p < 0.010$ ). In contrast, following expression of *Mtss1*-exon 12 in KO-granule cells does not appreciably affect neurite density (at DIV 6,  $p = 0.803$ ; at DIV 10,  $p = 0.058$  for transduced vs KO cells). Neurite density is expressed as the percentage of the area covered by MAP2 positive processes. Results are representative data of two independent experiments

Conversely, the persistence of such defects even after selective restoration of *Mtss1* to Purkinje cells indicates that *Mtss1* expression in Purkinje cell afferents is also required for orderly Purkinje cell dendritogenesis. A parsimonious explanation of this observation is that *Mtss1* deficiency in granule cells impairs the physiologic transsynaptic tuning of Purkinje cell dendritogenesis (Schilling et al. 1991a; Baptista et al. 1994; for a review see; Sotelo and Rossi 2013).

Thus, persistent Purkinje cell dendritic defects in *Mtss1*-null mice with *Mtss1* expression restored to Purkinje cells also point to a hitherto unknown effect of *Mtss1* on axonal, or presynaptic, development and/or function. Two additional findings reported here further support this conclusion. First, abnormal synaptic terminals of Purkinje cells in deep cerebellar nuclei of *Mtss1*-deficient animals are the direct evidence for an axonal effect of *Mtss1*. Indeed, this appears a cell-intrinsic effect, as it is abolished upon re-expression of *Mtss1* in Purkinje cells of *Mtss1*-null animals. Second, impaired neuritogenesis of *Mtss1*-null granule cells strongly suggests that axon formation of these cells is also *Mtss1*-dependent. This latter interpretation is borne out by the recent observation that spontaneous excitatory postsynaptic currents (mEPSC) in Purkinje cells are reduced in young *Mtss1*<sup>-/-</sup> mice (Saarikangas et al. 2015). To wit, this signifies either a decreased density or release probability of excitatory Purkinje cell afferents. Whether this axonal phenotype related to *Mtss1* expression implies sorting of this protein to the axon, or reflects an indirect, say an effect of *Mtss1* on the sorting of other constituents to the axon, is currently not known.

Our analysis of granule cell neuritogenesis *in vitro* provide one rationale to explain the morphological (this study) and electrophysiological (Saarikangas et al. 2015) changes indicative of a reduced granule cell innervation of Purkinje cells following *Mtss1* ablation. First, we note that any effect observed *in vitro* is unambiguously intrinsic to granule cells, since their postsynaptic targets, viz. Purkinje cells, do not survive in cerebellar cultures as used here (see e.g., Tabata et al. 2000). More importantly, our reconstitution experiments not only document that re-expression of *Mtss1* is necessary and sufficient to normalize neurite formation to the level seen in wild-type granule cells, but also that this is specific for the exon 12a variant of *Mtss1*. Consistently, the time course of expression of the cognate exon 12a variant parallels the phase of massive granule cell axon growth. These observations define a first function specific to the exon 12a variant of *Mtss1*, and in fact one that seems nicely compatible with the CNS-specific expression of this isoform, which is not found in peripheral tissues (Glassmann et al. 2007). Unfortunately, the structure of these exons do not suggest any reasonable clues how this specific function may be mechanistically realized (for a sequence

comparison of exons 12 and 12a and a discussion of potential consequences, see Glassmann et al. 2007).

### Orderly granule cell migration depends on *Mtss1*

The sub-meningeal granule cell ectopias observed *Mtss1*-deficient animals indicate that *Mtss1* also affects granule cell migration. While selective re-expression of *Mtss1* in Purkinje neurons does not appreciably affect granule cell ectopias in *Mtss1*-null animals, selective restoration of *Mtss1* to granule cell precursors on a null background greatly reduces the extent and numbers of such ectopias. In fact, persistent granule cell ectopias in *Mtss1*-null mice with re-expression of *Mtss1* in granule cell precursors are restricted to the posterior cerebellum, where the promoter used to reconstitute *Mtss1*-expression to granule cell precursors is known to be less efficient and turned on only later during development (Machold and Fishell 2005; Pan et al. 2009). Thus, this phenotype independently supports the conclusion that ectopias are caused primarily by *Mtss1* deficiency specifically in granule cell precursors. For the sake of completeness, we note that we cannot formally exclude that the proper granule cell migration may also be influenced on *Mtss1* expression also in non-granule cells, notably Purkinje neurons, though our data do not suggest such a conclusion. Quite to the contrary, the altered migratory behavior of *Mtss1*-null granule cells *in vitro* suggests a mechanistic interpretation of how *Mtss1* may cell-intrinsically impinge on granule cell motility.

The culture model used lacks typical directional cues that act on migrating granule cell *in situ*. Consistently, cultured wild-type granule cells move in an essentially random fashion, with only a minor degree of directional persistence. In contrast, mobility of *Mtss1*-deficient granule cells *in vitro* is hindered or corralled (Burov et al. 2011). Considering that *in vitro*, the predominant cell types which might impose corraling as observed in the absence of *Mtss1* are granule cells themselves, a tentative explanation for the origin of granule cell ectopias *in vivo* might be that *Mtss1* deficiency impedes the exit of early postmitotic granule cells from the EGL. This interpretation is in keeping with the established role for homotypic interactions of granule cells for their development (Gao et al. 1991), and it assigns *Mtss1* a cell-intrinsic function in this process.

Intriguingly, recent observations in bone marrow cells (Zhan et al. 2016) suggest that *Mtss1*-deficient granule cell precursors may be incapable to down-regulate *Cxcr4* surface expression. This, in consequence, may be predicted to impede the orderly emigration of differentiating granule cells from the external granule cell layer (Vilz et al. 2005), and thus suggests a granule cell-intrinsic, direct molecular mechanism to explain the phenotype observed here. Further, the known positive effects of *Mtss1* on *Rac1* activity



(Bompard et al. 2005; Suetsugu et al. 2006; Dawson et al. 2012a) may also contribute to explain the migratory deficits we observed in *Mtss1*-null granule cells. Active Rac1 positively regulates granule cell polarization and migration by modulating actin dynamics (Tahirovic et al. 2010). Intriguingly, Purkinje cell spine development and axon arborisation are also the subject to Rac1 activity (cf Luo et al. 1996). Similarly, a direct interaction between *Mtss1* and RhoA has been observed in cancer cells, resulting in a reduction of Rho activity (Mertz et al. 2014; Lei et al. 2014). Interestingly, RhoA-deficient cerebellar granule cells exhibit delayed migration (Mulherkar et al. 2014). Lastly, *Mtss1* has recently also been described to scaffold and organize aPKC- $\lambda$ , Pard3, and Pard6 (Atwood et al. 2013), which are known to regulate directional migration (Atwood et al. 2013; Crespo et al. 2014), including that of granule cells (Solecki et al. 2004). Together with the present results, these findings emphasize the concept that *Mtss1* provides a scaffold to integrate the fine-tuning of actin dynamics by multiple signaling cascades which assure proper granule cell migration.

Finally, the exon 12a-specific effect of *Mtss1* on granule cell neuritogenesis described above begs the question whether *Mtss1* effects on migration might be also exon-dependent. Experiments to address this issue are currently not feasible, as cultured granule cells become immobile and differentiate well before viral expression becomes efficient (Trenkner et al. 1984; Tarnok et al. 2005).

#### ***Mtss1* deficiency and protracted neuronal demise: a paradigm chronic neurodegeneration based on minimal developmental defects?**

A feature that distinguishes the cerebellar phenotype of *Mtss1*-deficient animals from other mutants with abnormalities in this brain region (e.g., Caviness and Rakic 1978; Manzano et al. 2007; Fernandez-Gonzalez et al. 2002; Kullmann et al. 2012) is the rather protracted and progressive demise of Purkinje cells and the accompanying neurological deficits as documented here, and also by Saarikangas et al. (2015), who used a genetically different *Mtss1*-deficient strains of mice than the one analyzed here. This loss of neurons, superimposed on a clear-cut developmental disruption, also distinguishes *Mtss1*-deficient animals from mice in which other I-BAR (Sawallisch et al. 2009; Kim et al. 2009) or F-BAR proteins (Carlson et al. 2011; Charrier et al. 2012) have been ablated.

Intriguingly, the observation that Purkinje cell loss is greatly reduced if *Mtss1* expression is selectively restored to Purkinje cells (on an otherwise *Mtss1*-null background) allows to separate the effects of *Mtss1* on Purkinje cell survival and dysmorphology. The latter

cannot be the sole cause of the protracted neurological demise observed in globally *Mtss1*-null animals. This focuses attention on the nuclear localization of *Mtss1* seen in older animals and raises the question whether *Mtss1* affects nuclear organization and, eventually, transcriptional dynamics. For one, the lipid composition of the nuclear membrane [for a review, see (Barlow et al. 2010)] is such that it would allow *Mtss1* to bind (Mattila et al. 2007). Further, recent research has revealed increasing evidence for the presence and regulatory function of actin within the nucleus (for reviews, see Treisman 2013; Hendzel 2014). Whether *Mtss1* acts within the nucleus in an analogous mode as at the cell membrane, or in a hitherto unknown fashion, remains to be seen. Still, the present data clearly identify *Mtss1* as member of a growing number of actin-interacting proteins with (regulated) nuclear location which may be critical to regulating actin nuclear function(s) (see, e.g., Johnson et al. 2013 and further references therein). Of note, our observation that the exon 12 variant of *Mtss1*, but not the variant comprising exon 12a, may enter the nucleus suggests that nuclear access of *Mtss1* is developmentally regulated, in parallel with splicing. Finally, as the nuclear localization and export signals encoded in the *Mtss1* sequence are not affected by differential usage of exons 12 or 12a (Glassmann et al. 2007), we may conclude that exon 12a constitutes a structural hindrance for nuclear entry.

In conclusion, the present results provide a detailed account of the function of *Mtss1*, a key linker between the actin cytoskeleton and the cell membrane, for the development and maintenance of a paradigmatic neuronal circuit, the cerebellar cortex. We identify cellular sites of action responsible for the pleiotropic effects of this protein on cell survival, migration, and neuritogenesis. Further, our data identify a specific effect of the *Mtss1*-exon 12a splice variant on neuritogenesis and thus identify a first function for this so far enigmatic neuron-specific isoform. Lastly, the protracted neurodegeneration seen in *Mtss1*-null mice suggests them as a model to study the linkage between neurodevelopmental disorders and neurodegeneration.

**Acknowledgements** We gratefully acknowledge the generous gift of *Mtss1*-deficient animals by Dr. Rong Li; of *Atoh1*-cre animals by Dr. Ulrich Schüller and *Pcp2*-cre mice by Dr. Michael Meyer. We are greatly indebted to Andrea Christ and Helma Langmann for excellent technical assistance, Daniela Krauss and Narziss Haias for invaluable help with animal husbandry; Alexander Glassmann and Kirsten Knapp for providing plasmids containing *Mtss1*-cDNA, and to Benjamin Odermatt for many constructive discussions.

#### **Compliance with ethical standards**

**Conflict of interest** The authors declare that they have no conflict of interest.

## References

- Altman J, Anderson WJ (1972) Experimental reorganization of the cerebellar cortex. I. Morphological effects of elimination of all microneurons with prolonged x-irradiation started at birth. *J Comp Neurol* 146:355–405
- Atwood SX, Li M, Lee A, Tang JY, Oro AE (2013) GLI activation by atypical protein kinase C  $\iota/\lambda$  regulates the growth of basal cell carcinomas. *Nature* 494:484–488
- Baptista CA, Hatten ME, Blazeski R, Mason CA (1994) Cell-cell interactions influence survival and differentiation of purified Purkinje cells in vitro. *Neuron* 12:243–260
- Barlow CA, Laishram RS, Anderson RA (2010) Nuclear phosphoinositides: a signaling enigma wrapped in a compartmental conundrum. *Trends Cell Biol* 20:25–35
- Barski JJ, Dethleffsen K, Meyer M (2000) Cre recombinase expression in cerebellar Purkinje cells. *Genesis* 28:93–98
- Ben-Arie N, Bellen HJ, Armstrong DL, McCall AE, Gordatzke PR, Guo Q, Matzuk MM, Zoghbi HY (1997) *Math1* is essential for genesis of cerebellar granule neurons. *Nature* 390:169–172
- Bompard G, Sharp SJ, Freiss G, Machesky LM (2005) Involvement of Rac in actin cytoskeleton rearrangements induced by MIM-B. *J Cell Sci* 118:5393–5403
- Burov S, Jeon JH, Metzler R, Barkai E (2011) Single particle tracking in systems showing anomalous diffusion: the role of weak ergodicity breaking. *Phys Chem Chem Phys* 13:1800–1812
- Carlson BR, Lloyd KE, Kruszewski A, Kim IH, Rodriguiz RM, Heindel C, Faytell M, Dudek SM, Wetsel WC, Soderling SH (2011) WRP/srGAP3 facilitates the initiation of spine development by an inverse F-BAR domain, and its loss impairs long-term memory. *J Neurosci* 31:2447–2460
- Caviness VS Jr, Rakic P (1978) Mechanisms of cortical development: a view from mutations in mice. *Annu Rev Neurosci* 1:297–326
- Charrier C, Joshi K, Coutinho-Budd J, Kim JE, Lambert N, de MJ, Jin WL, Vanderhaeghen P, Ghosh A, Sassa T, Polleux F (2012) Inhibition of SRGAP2 function by its human-specific paralogs induces neoteny during spine maturation. *Cell* 149:923–935
- Crespo CL, Vernieri C, Keller PJ, Garre M, Bender JR, Wittbrodt J, Pardi R (2014) The PAR complex controls the spatiotemporal dynamics of F-actin and the MTOC in directionally migrating leukocytes. *J Cell Sci* 127:4381–4395
- Da Silva JS, Dotti CG (2002) Breaking the neuronal sphere: regulation of the actin cytoskeleton in neurogenesis. *Nat Rev Neurosci* 3:694–704
- Dawson JC, Bruche S, Spence HJ, Braga VM, Machesky LM (2012a) *Mtss1* promotes cell-cell junction assembly and stability through the small GTPase Rac1. *PLoS ONE* 7:e31141
- Dawson JC, Timpson P, Kalna G, Machesky LM (2012b) *Mtss1* regulates epidermal growth factor signaling in head and neck squamous carcinoma cells. *Oncogene* 31:1781–1793
- Dickinson RB, Tranquillo RT (1993) Optimal estimation of cell movement indices from the statistical analysis of cell tracking data. *AICHE J* 39:1995–2010.
- Fernandez-Gonzalez A, La Spada AR, Treadaway J, Higdon JC, Harris BS, Sidman RL, Morgan JI, Zuo J (2002) Purkinje cell degeneration (*pcd*) phenotypes caused by mutations in the axotomy-induced gene, *Nna1*. *Science* 295:1904–1906
- Flynn KC (2013) The cytoskeleton and neurite initiation. *Bioarchitecture* 3:86–109
- Gao WQ, Heintz N, Hatten ME (1991) Cerebellar granule cell neurogenesis is regulated by cell-cell interactions in vitro. *Neuron* 6:705–715
- Glassmann A, Molly S, Surchev L, Nazwar TA, Holst M, Hartmann W, Baader SL, Oberdick J, Pietsch T, Schilling K (2007) Developmental expression and differentiation-related neuron-specific splicing of metastasis suppressor 1 (*Mtss1*) in normal and transformed cerebellar cells. *BMC Dev Biol* 7:111
- Hayn-Leichsenring G, Liebig C, Miething A, Schulz A, Kumar S, Schwalbe M, Eiberger B, Baader SL (2011) Cellular distribution of metastasis suppressor 1 and the shape of cell bodies are temporarily altered in *Engrailed-2* overexpressing cerebellar Purkinje cells. *Neuroscience* 189:68–78
- Hendzel MJ (2014) The F-act's of nuclear actin. *Curr Opin Cell Biol* 28:84–89
- Hothorn T, Bretz F, Westfall P (2008) Simultaneous inference in general parametric models. *Biom J* 50:346–363
- Johnson MA, Sharma M, Mok MT, Henderson BR (2013) Stimulation of in vivo nuclear transport dynamics of actin and its co-factors IQGAP1 and Rac1 in response to DNA replication stress. *Biochim Biophys Acta* 1833:2334–2347
- Kim MH, Choi J, Yang J, Chung W, Kim JH, Paik SK, Kim K, Han S, Won H, Bae YS, Cho SH, Seo J, Bae YC, Choi SY, Kim E (2009) Enhanced NMDA receptor-mediated synaptic transmission, enhanced long-term potentiation, and impaired learning and memory in mice lacking *IRSp53*. *J Neurosci* 29:1586–1595
- Kullmann JA, Neumeier A, Wickertsheim I, Bottcher RT, Costell M, Deitmer JW, Witke W, Friauf E, Rust MB (2012) Purkinje cell loss and motor coordination defects in *profilin1* mutant mice. *Neuroscience* 223:355–364
- Lee YG, Macoska JA, Korenchuk S, Pienta KJ (2002) MIM, a potential metastasis suppressor gene in bladder cancer. *Neoplasia* 4:291–294
- Lei R, Tang J, Zhuang X, Deng R, Li G, Yu J, Liang Y, Xiao J, Wang HY, Yang Q, Hu G (2014) Suppression of MIM by micro-RNA-182 activates RhoA and promotes breast cancer metastasis. *Oncogene* 33:1287–1296
- Leto K, Arancillo M, Becker EB, Buffo A, Chiang C, Ding B, Dobyns WB, Dusart I, Haldipur P, Hatten ME, Hoshino M, Joyner AL, Kano M, Kilpatrick DL, Koibuchi N, Marino S, Martinez S, Millen KJ, Millner TO, Miyata T, Parmigiani E, Schilling K, Sekerkova G, Sillitoe RV, Sotelo C, Uesaka N, Wefers A, Wingate RJ, Hawkes R (2016) Consensus paper: cerebellar development. *Cerebellum* 15:789–828
- Luo L, Hensch TK, Ackerman L, Barbel S, Jan LY, Jan YN (1996) Differential effects of the Rac GTPase on Purkinje cell axons and dendritic trunks and spines. *Nature* 379:837–840
- Machold RP, Fishell G (2005) *Math1* is expressed in temporally discrete pools of cerebellar rhombic-lip neural progenitors. *Neuron* 48:17–24
- Manzano J, Cuadrado M, Morte B, Bernal J (2007) Influence of thyroid hormone and thyroid hormone receptors in the generation of cerebellar gamma-aminobutyric acid-ergic interneurons from precursor cells. *Endocrinology* 148:5746–5751
- Marin O, Rubenstein JL (2003) Cell migration in the forebrain. *Annu Rev Neurosci* 26:441–483
- Matei V, Pauley S, Kaing S, Rowitch D, Beisel KW, Morris K, Feng F, Jones K, Lee J, Fritzsche B (2005) Smaller inner ear sensory epithelia in *Neurog 1* null mice are related to earlier hair cell cycle exit. *Dev Dyn* 234:633–650
- Mattila PK, Salminen M, Yamashiro T, Lappalainen P (2003) Mouse MIM, a tissue-specific regulator of cytoskeletal dynamics, interacts with ATP-actin monomers through its C-terminal WH2 domain. *J Biol Chem* 278:8452–8459
- Mattila PK, Pykalainen A, Saarikangas J, Paavilainen VO, Vihinen H, Jokitalo E, Lappalainen P (2007) Missing-in-metastasis and *IRSp53* deform PI(4,5)P<sub>2</sub>-rich membranes by an inverse BAR domain-like mechanism. *J Cell Biol* 176:953–964
- McClure C, Cole KL, Wulff P, Klugmann M, Murray AJ (2011) Production and titration of recombinant adeno-associated viral vectors. *J Vis Exp* 57:e3348

- Mertz KD, Pathria G, Wagner C, Saarikangas J, Sboner A, Romanov J, Gschaidner M, Lenz F, Neumann F, Schreiner W, Nemethova M, Glassmann A, Lappalainen P, Stingl G, Small JV, Fink D, Chin L, Wagner SN (2014) MTSS1 is a metastasis driver in a subset of human melanomas. *Nat Commun* 5:3465
- Metin C, Vallee RB, Rakic P, Bhide PG (2008) Modes and mishaps of neuronal migration in the mammalian brain. *J Neurosci* 28:11746–11752
- Metzler R, Klafter J (2000) The random walk's guide to anomalous diffusion: a fractional dynamics approach. *Phys Rep* 339:1–77.
- Michalet X (2010) Mean square displacement analysis of single-particle trajectories with localization error: Brownian motion in an isotropic medium. *Phys Rev E Stat Nonlin Soft Matter Phys* 82:041914
- Mulherkar S, Uddin MD, Couvillon AD, Sillitoe RV, Tolias KF (2014) The small GTPases RhoA and Rac1 regulate cerebellar development by controlling cell morphogenesis, migration and foliation. *Dev Biol* 394:39–53
- Newman AJ, Tremblay A, Nichols ES, Neville HJ, Ullman MT (2011) The influence of language proficiency on lexical semantic processing in native and late learners of english. *J Cogn Neurosci* 24:1205–1223
- Oberdick J, Smeyne RJ, Mann JR, Zackson S, Morgan JI (1990) A promoter that drives transgene expression in cerebellar Purkinje and retinal bipolar neurons. *Science* 248:223–226
- Pan N, Jahan I, Lee JE, Fritzsche B (2009) Defects in the cerebella of conditional Neurod1 null mice correlate with effective Tg(Atoh1-cre) recombination and granule cell requirements for Neurod1 for differentiation. *Cell Tissue Res* 337:407–428
- Pfaffl MW (2001) A new mathematical model for relative quantification in real-time RT-PCR. *Nucleic Acids Res* 29:2002–2007
- R Core Team (2015) R: A language and environment for statistical computing. Vienna, Austria: R Foundation for Statistical Computing ISBN 3-900051-07-0; <http://www.R-project.org/>.
- Rakic P (1988) Specification of cerebral cortical areas. *Science* 241:170–176
- Ruthardt N, Lamb DC, Brauchle C (2011) Single-particle tracking as a quantitative microscopy-based approach to unravel cell entry mechanisms of viruses and pharmaceutical nanoparticles. *Mol Ther* 19:1199–1211
- Saarikangas J, Mattila PK, Varjosalo M, Bovellan M, Hakanen J, Calzada-Wack J, Tost M, Jennen L, Rathkolb B, Hans W, Horsch M, Hyvonen ME, Perala N, Fuchs H, Gailus-Durner V, Esposito I, Wolf E, De Angelis MH, Frilander MJ, Savilahti H, Sariola H, Sainio K, Lehtonen S, Taipale J, Salminen M, Lappalainen P (2011) Missing-in-metastasis MIM/MTSS1 promotes actin assembly at intercellular junctions and is required for integrity of kidney epithelia. *J Cell Sci* 124:1245–1255
- Saarikangas J, Kourdougli N, Senju Y, Chazal G, Segerstrale M, Minkeviciene R, Kuurne J, Mattila PK, Garrett L, Holter SM, Becker L, Racz I, Hans W, Klopstock T, Wurst W, Zimmer A, Fuchs H, Gailus-Durner V, Hrabe de AM, von OL, Taira T, Lappalainen P, Rivera C, Hotulainen P (2015) MIM-induced membrane bending promotes dendritic spine initiation. *Dev Cell* 33:644–659
- Sawallisch C, Berhorster K, Disanza A, Mantoani S, Kintscher M, Stoenica L, Dityatev A, Sieber S, Kindler S, Morellini F, Schweizer M, Boeckers TM, Korte M, Scita G, Kreienkamp HJ (2009) The insulin receptor substrate of 53 kDa (IRSp53) limits hippocampal synaptic plasticity. *J Biol Chem* 284:9225–9236
- Schilling K, Dickinson MH, Connor JA, Morgan JI (1991a) Electrical activity in cerebellar cultures determines Purkinje cell dendritic growth patterns. *Neuron* 7:891–902
- Schilling K, Luk D, Curran T, Morgan JI (1991b) Regulation of a fos-lacZ fusion gene: a paradigm for quantitative analysis of stimulus-transcription coupling. *Proc Natl Acad Sci USA* 88:5665–5669
- Solecki DJ, Model L, Gaetz J, Kapoor TM, Hatten ME (2004) Par-1alpha signaling controls glial-guided neuronal migration. *Nat Neurosci* 7:1195–1203
- Sotelo C, Rossi F (2013) Purkinje cell migration and differentiation. In: Manto M, Gruol DL, Schmahmann JD, Koibuchi N, Rossi F (eds) *Handbook of the cerebellum and cerebellar disorders*. Springer, New York, pp 147–178
- Suetsugu S (2010) The proposed functions of membrane curvatures mediated by the BAR domain superfamily proteins. *J Biochem* 148:1–12
- Suetsugu S, Murayama K, Sakamoto A, Hanawa-Suetsugu K, Seto A, Oikawa T, Mishima C, Shirouzu M, Takenawa T, Yokoyama S (2006) The RAC binding domain/IRSp53-MIM homology domain of IRSp53 induces RAC-dependent membrane deformation. *J Biol Chem* 281:35347–35358
- Suetsugu S, Kurisu S, Takenawa T (2014) Dynamic shaping of cellular membranes by phospholipids and membrane-deforming proteins. *Physiol Rev* 94:1219–1248
- Tabata T, Sawada S, Araki K, Bono Y, Furuya S, Kano M (2000) A reliable method for culture of dissociated mouse cerebellar cells enriched for Purkinje neurons. *J Neurosci Methods* 104:45–53
- Tahirovic S, Hellal F, Neukirchen D, Hindges R, Garvalov BK, Flynn KC, Stradal TE, Chrostek-Grashoff A, Brakebusch C, Bradke F (2010) Rac1 regulates neuronal polarization through the WAVE complex. *J Neurosci* 30:6930–6943
- Tarnok K, Czirik A, Czondor K, Schlett K (2005) Cerebellar granule cells show age-dependent migratory differences in vitro. *J Neurobiol* 65:135–145
- Treisman R (2013) Shedding light on nuclear actin dynamics and function. *Trends Biochem Sci* 38:376–377
- Trenkner E, Smith D, Segil N (1984) Is cerebellar granule cell migration regulated by an internal clock? *J Neurosci* 4:2850–2855
- Van Dine SE, Siu NY, Toia A, Cuoco JA, Betz AJ, Bolivar VJ, Torres G, Ramos RL (2015) Spontaneous malformations of the cerebellar vermis: Prevalence, inheritance, and relationship to lobule/fissure organization in the C57BL/6 lineage. *Neuroscience* 310:242–251
- Vilz TO, Moepps B, Engele J, Molly S, Littman DR, Schilling K (2005) The SDF-1/CXCR4 pathway and the development of the cerebellar system. *Eur J Neurosci* 22:1831–1839
- Weyer A, Schilling K (2003) Developmental and cell type-specific expression of the neuronal marker NeuN in the murine cerebellum. *J Neurosci Res* 73:400–409
- Xia S, Li X, Johnson T, Seidel C, Wallace DP, Li R (2010) Polycystin-dependent fluid flow sensing targets histone deacetylase 5 to prevent the development of renal cysts. *Development* 137:1075–1084.
- Zhan T, Cao C, Li L, Gu N, Civin CI, Zhan X (2016) MIM regulates the trafficking of bone marrow cells via modulating surface expression of CXCR4. *Leukemia* 30:1327–1334